EG&G Idaho, Inc.

FORM EG&G-398
(Rev. 11-79)

8005140140

INTERIM REPORT

Accession No. _____

Report No. EGG-TFBP-5122

Contract Program or Project Title: Thermal Fuels Behavior Program

Subject of this Document: Power-Cooling-Mismatch Test Series Test PR-1 Quick Look Report

Type of Document: Quick Look Report

Author(s): D. T. Sparks, F. S. Gunnerson, Z. R. Martinson, N. T. LeFebre

Date of Document: March 1980

Responsible NRC Individual and NRC Office or Division: M. L. Picklesimer

EG&G Idaho, Inc.
Idaho Falls, Idaho 83415

Prepared for the
U.S. Nuclear Regulatory Commission
Washington, D.C.
Under DOE Contract No. DE-AC07-76ID01570
NRC FIN No. A6041

INTERIM REPORT

EGG-TFBP-5122

March 1980

POWER-COOLING-MISMATCH TEST SERIES TEST PR-1

QUICK LOOK REPORT

D. T. Sparks
F. S. Gunnerson
Z. R. Martinson
N. T. LeFebre

U.S. Department of Energy
Idaho Operations Office • Idaho National Engineering Laboratory

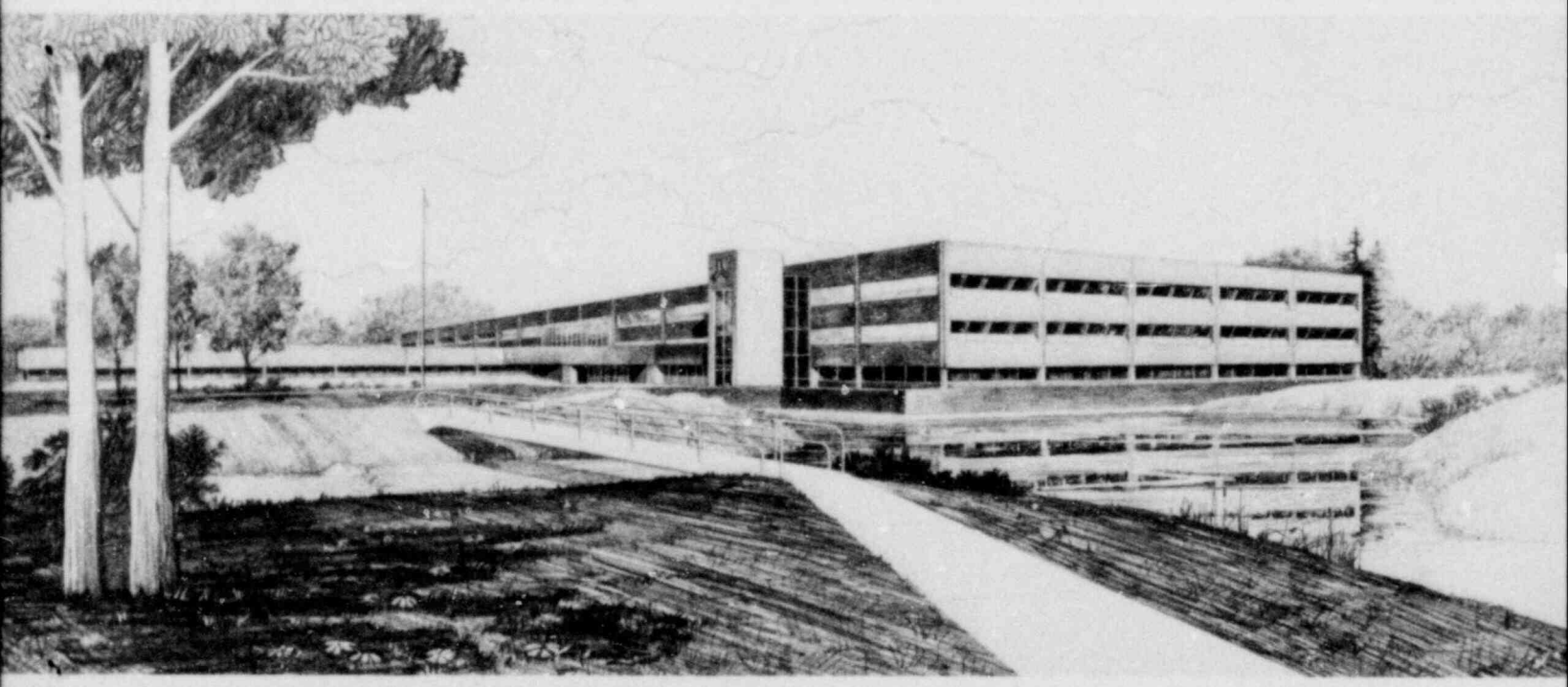

This is an informal report intended for use as a preliminary or working document

Prepared for the
U.S. Nuclear Regulatory Commission
Under DOE Contract No. DE-AC07-76ID01570
FIN No. A6041

EG&G Idaho

SUMMARY

A combination power-cooling-mismatch (PCM) and reactivity initiated accident (RIA) experiment was performed as part of the Thermal Fuels Behavior Program Conducted by EG&G Idaho, Inc., for the U. S. Nuclear Regulatory Commission. This test, designated Test PR-1, was one of a series of in-pile experiments designed to investigate the behavior of light water reactor type fuel rods under steady state and transient operating conditions. The original objective of Test PR-1 was to provide fuel rod thermal response information under steady state and power oscillation conditions, in support of previous gap conductance testing in the Power Burst Facility (PBF). The test objective was subsequently expanded to include investigation of the conditions at onset of boiling transition, the conditions at return to nucleate boiling or quench, the potential for two-phase hydrodynamic instabilities, and fuel temperature distributions and rod failure limits during RIA power excursions. The preliminary results from Test PR-1 are presented in this report.

Test PR-1 was conducted with four unirradiated boiling water reactor (BWR) type fuel rods, each 0.914-m in length. The rods were contained within individual coolant flow shrouds (hydraulically coupled through common upper and lower plenums) and backfilled to a cold internal pressure of 2.58 MPa with either helium (3 rods) or argon (1 rod) gas. Fuel densities in the helium filled test rods were 92, 95, and 97% of theoretical density to provide a direct evaluation of fuel density on fuel rod thermal response.

Test PR-1 included three test phases: a steady state and power oscillation phase to evaluate fuel rod thermal response; a PCM transient testing phase to evaluate the conditions at onset of boiling transition, return to nucleate boiling, and the potential for two-phase hydrodynamic instabilities; and, an RIA power excursion phase to investigate fuel temperature distributions and provide information on fuel rod failure limits during RIA power excursions.

The thermal response data obtained during Test PR-1 complement similar data from previous gap conductance (GC) test series experiments. Since the Test PR-1 hardware was originally designed for a GC series experiment,

instrumentation on the fuel rods was optimally positioned for thermal response measurements. The effect of fuel density variations in the helium filled test rods was expected to be small on the basis of previous test results. Minor variations were detected in centerline and off-center fuel temperatures between the helium filled rods but may be associated with uncertainties in the measurements, rather than effects due to fuel density variations. The effect of fill gas composition, however, was pronounced. As expected, fuel temperatures in the argon filled rod were noticeably higher than the helium filled rods due to the lower thermal conductivity of argon.

Power-cooling-mismatch transients were conducted at system pressures between 7 and 15.5 MPa, with test rod peak powers between 40 and 53 kW/m. A total of seven flow reduction transients (each at constant test rod power) were conducted at low pressures, between 7 and 8 MPa, at a coolant inlet temperature of about 544 K. No discernible indications of boiling transition were observed. Either natural circulation was sufficient to preclude boiling transition, or the low temperature excursion associated with a high quality dryout transition was not detectable with the Test PR-1 instrumentation.

Eighteen PCM-type transients were conducted at system pressures between 13 and 15.5 MPa. The coolant inlet temperature at each pressure was adjusted to provide a nearly constant inlet subcooling (~14 K). At least thirteen of the transients resulted in detectable boiling transition on the rods. Rewet was induced by three methods: (a) increasing flow and decreasing power simultaneously, (b) increasing flow rate at constant power, or (c) decreasing power at constant flow rate. One rod, Rod 524-1, failed during the boiling transition cycles. The rod likely failed due to embrittlement following extended high temperature operation.

During the final test phase, progressively severe RIA power excursions were performed at radial average fuel enthalpies at the peak power elevation of 105, 125, and 180 cal/g UO_2. Reactor periods to attain these energies were 42.7, 8.7 and 6.2 ms, respectively. During the two higher energy bursts, fuel temperatures did not increase as rapidly as predicted from pretest calculations. Such behavior may be associated with the thermocouple response time rather than an inherent delay in temperature increase. Film boiling was

observed following each power burst with measured cladding temperatures at the peak power elevation of 1950 K following the highest energy burst. The pressure transducer data from Rod 524-2 indicated rod failure during the final (highest energy) power burst. The cladding displacement measurement on Rod 524-3 may have indicated rod failure during the second (125 cal/g) power burst. The argon filled test rod, Rod 524-4, did not fail during the power excursions. Measured cladding temperatures on Rod 524-4 were about 700 K less than on the helium filled test rods (at common elevations) during the highest energy power burst.

CONTENTS

FIGURES

TABLES

1. INTRODUCTION

To interpret the behavior of light water reactor fuel rods during postulated accident events requires an understanding of the phenomena, and an ability to model the processes which dominate fuel rod response during such events. To license a light water reactor requires that the applicant ensure either that adequate thermal margin [illegible] allay the consequences of such an accident scenario, or ensure on the basis of an acceptable damage criteria that significant damage would not occur. The Power-Cooling-Mismatch Test series is being conducted in the Power Burst Facility (PBF) for the U.S. Nuclear Regulatory Commission to provide modeling and damage information on a spectrum of power cooling imbalance events. Data from the test series will be used to help evaluate conservatisms in the current thermal margin criteria, and provide input data for development and assessment of computer models used to calculate fuel rod response under a range of transient conditions.

Test PR-1 was originally designed to provide fuel rod thermal response data under steady state and power oscillation conditions. The test objectives were subsequently expanded to include boiling transition and return to nucleate boiling information under power-cooling-mismatch conditions, and fuel temperature distributions during RIA power excursions.

Test PR-1 was performed with four BWR-type fuel rods (each within a separate coolant flow shroud) symetrically positioned within the PBF in-pile tube. The test rods were backfilled with either helium (three rods) or argon (one rod) to a cold pressure of 2.58 MPa. The fuel density of the helium rods was varied to 92, 95, or 97% of theoretical. With this design, the effects of fuel density and gas composition on fuel rod thermal response were examined.

The conduct of Test PR-1 consisted of three phases. The first phase included 13.5 hours of steady state operation and 12.5 hours of power oscillations to obtain fuel rod thermal response data. The second phase consisted of 23 flow reduction and 2 power increase PCM transients. The transients provided boiling transition and return to nucleate boiling information at high pressure conditions (13 and 15.5 MPa system pressures), and data to evaluate the potential for two-phase instabilities in the Test

PR-1 4-rod geometry. The third phase consisted of three RIA power excursions initiated from BWR hot startup conditions to evaluate fuel temperature distributions and provide data on rod failure limits during RIA power excursions. The power excursions were progressively severe, with radial average fuel enthalpies at the axial peak elevation of 105, 125 and 180 cal/g UO_2.

A description of the experiment design and conduct is presented in Section 2. The fuel rod thermal response during Test PR-1 is described in Section 3. Interpretation of the PCM and boiling transition results are discussed in Section 4. Results from the RIA power excursions are contained in Section 5. Results and observations from Test PR-1 are summarized in Section 6.

2. EXPERIMENT DESIGN AND CONDUCT

Test PCM-RIA-1 (PR-1) was conducted to provide fuel rod thermal response data under steady state and transient conditions, to obtain information on conditions at onset of boiling transition and return to nucleate boiling, and to evaluate fuel temperature distributions and failure thresholds under RIA power burst conditions. A description of the Experiment Design and an account of the Experiment Conduct are presented in this section.

2.1 Experiment Design

The Test PR-1 hardware was originally designed for the Gap Conductance test series, with the objective of obtaining steady state and transient fuel rod thermal response information. The objectives of the test were subsequently expanded to include boiling transition and quench data during power-cooling-mismatch (PCM) transients, and fuel temperature distributions during a series of reactivity initiated accident (RIA) power excursions.

2.1.1 Fuel Rods and Flow Shroud. Test PR-1 was conducted with four, BWR-type test fuel rods identified as Rods 524-1, 524-2, 524-3, and 524-4. The active fuel length of each test rod was 0.914 m and the plenum volume was sized in proportion to the active fuel volume. Rods 524-1, 524-2, and 524-3 were backfilled with helium, and Rod 524-4 was backfilled with argon to allow comparison of the effect of fill gas composition upon fuel rod thermal response. The fuel density of the four test rods was also varied to provide comparative data for determining the effect of fuel density during each phase of the test. The individual fuel rod design characteristics are listed in Table 1. The orientations of the test rods in the 4-rod hardware, and the relative azimuthal and axial locations of the fuel rod instrumentation are shown in Figure 1.

Each test rod was instrumented with thermocouples to measure cladding surface temperature, fuel pellet centerline temperature, and off-center fuel temperature. In addition, Rod 524-4 was instrumented with cladding internal thermocouples to provide information on rewetting from film boiling conditions. The internal pressure in each rod upper plenum was measured by a pressure transducer.

TABLE 1. NOMINAL DESIGN PARAMETERS OF BWR-TYPE FUEL RODS FOR TEST PR-1

Rod Parameter	Value
Cladding outside diameter (mm)	12.50
Cladding inside diameter (mm)	10.79
Wall thickness (mm)	0.86
Cladding material	Zr-2
Fuel material	UO_2
Fuel density (% theoretical density)	95 (Rod 524-1), 92 (Rod 524-2), 97 (Rod 524-3), 97 (Rod 524-4)
Pellet diameter (mm)	10.57
Initial diametral gap (mm)	0.22[a]
Fill gas composition	helium (Rods 524-1,-2, and -3), argon (Rod 524-4)
Internal pressure (MPa)	2.58
Pellet enrichment (wt% U-235)	10
Pellet shape	Flat ends L/D = 1.0
Pellet length (mm)	10.57
Rod overall length (mm)	990.6
Fuel stack length (mm)	914.4
Plenum length (mm)	55.12
Plenum vol/fuel vol ratio	0.08
Plenum spring	Coiled Carbon Steel
Shroud inside diameter (mm)	19.3

a. Corresponds to 2.2% of initial fuel pellet diameter.

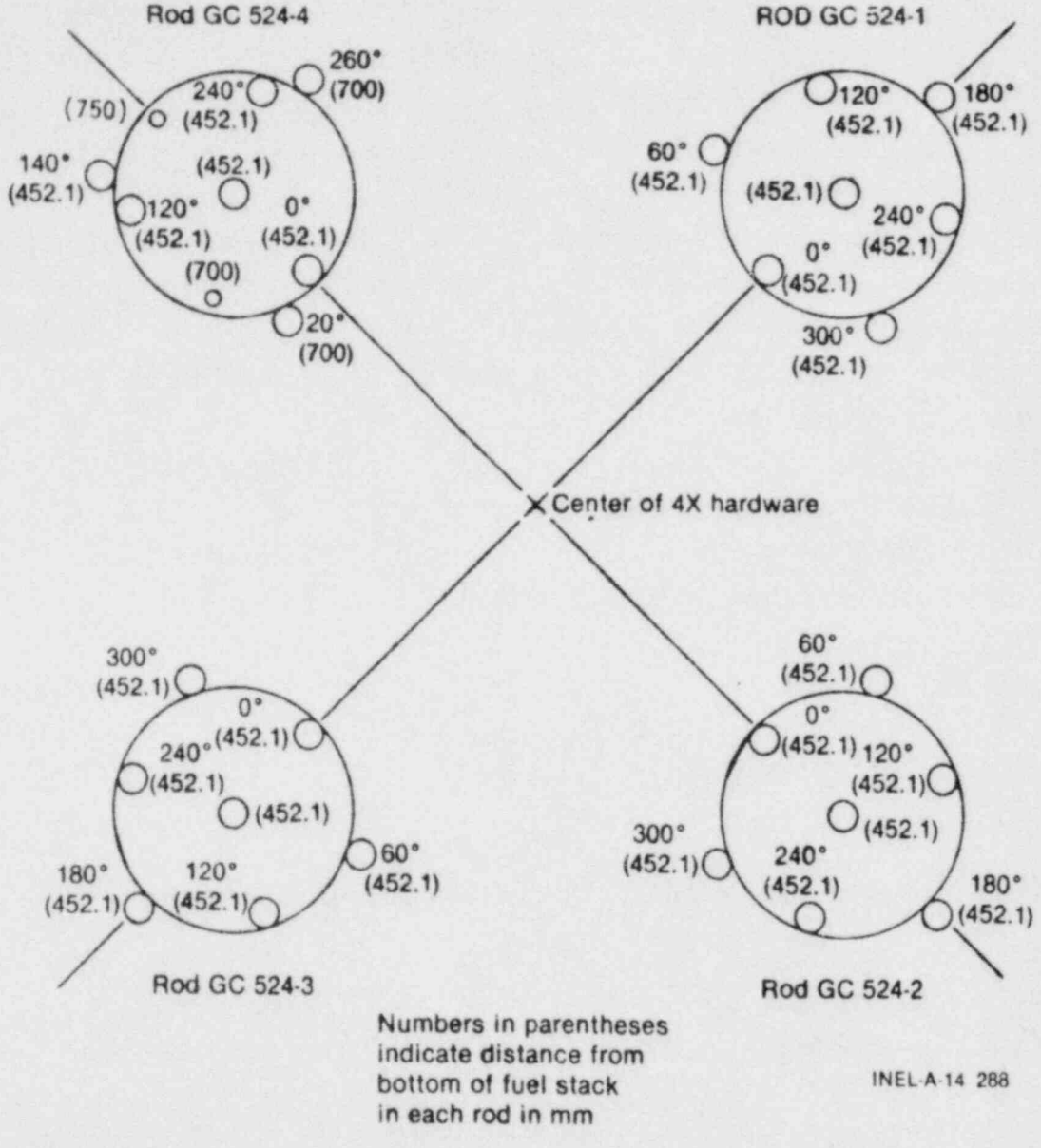

Figure 1. Four rod orientation and relative fuel rod instrumentation locations for Test PR-1.

The rods were positioned within individual coolant flow shrouds to thermally isolate the rods within the test train. Each shroud was constructed of zircaloy with a 19.3 mm inside diameter, and positioned symmetrically within the PBF in-pile tube (IPT). The instrumentation associated with each fuel rod flow shroud consisted of: an inlet turbine flowmeter located in each lower shroud extension to measure the coolant volumetric flow rate; differential thermocouples mounted at each shroud inlet and outlet to measure the coolant temperature increase through the flow shroud; thermocouples located at the inlet and outlet of each flow shroud to measure coolant inlet and outlet temperature; and a differential pressure transducer attached to the top and bottom of the flow shrouds on Rods 524-3 and 524-4 to measure pressure drop across the rod heated length. The recorded data from these instruments were used to calculate fuel rod power and for monitoring coolant environmental parameters. A linear variable differential transformer (LVDT) to measure cladding elongation was attached to the lower end of each flow shroud. Flux wires to measure the relative axial and azimuthal power profiles were attached to each flow shroud.

2.1.2 Test Train. The test train supported the four fuel rods symmetrically about the central axis of the in-pile tube. The center hanger rod and lower support plate provided the principal structural support for the fuel train.

The coolant entered the IPT at the inlet and was directed through the downcomer to the lower plenum. The flow was subsequently directed upward through the catch basket, through the test rod flow shrouds, and into the upper plenum. Some lower plenum flow bypassed the lower support and entered the bypass region outside the individual flow shrouds. The coolant exited the IPT at the outlet.

The instrumentation associated with the test train consisted of: pressure transducers mounted near the shroud outlets to measure coolant pressure, and self-powered neutron detectors mounted on supports outside the flow shrouds to measure relative thermal neutron flux.

2.1.3 Plant System. The PBF primary loop, shown in Figure 2, consisted of: a pressurizer, coolant pump, coolant heater, heat exchanger, bypass line,

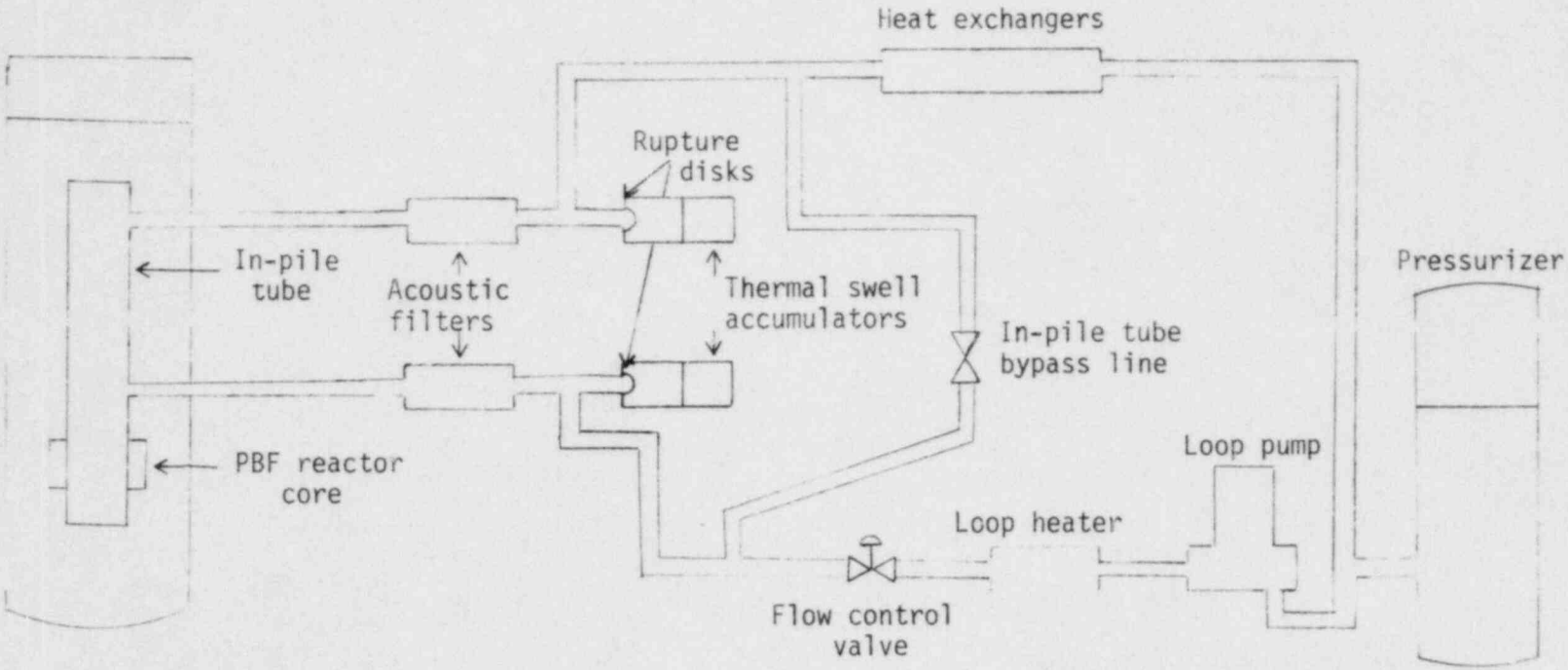

Figure 2. Schematic of PBF test loop and in-pile tube.

and in-pile tube. The loop coolant system provided the capability to monitor and control environmental coolant conditions and flow rate during test conduct.

Plant instrumentation to monitor coolant parameters during the test consisted of: a differential pressure transducer to measure pressure changes across the in-pile tube; an Ashcroft (Heise) loop pressure gauge; six pressure transducers located at various positions within the loop; and a Venturi loop flowmeter to measure the total loop flow rate. Nine ion chambers located in the PBF core region were used to measure reactor power. Flux wires were installed in both the reflector and fuel regions of the reactor core to determine the axial power profile.

2.2 Experiment Conduct

Test PR-1 was conducted to assess fuel rod response during various steady state and transient operating conditions. These conditions included; (a) operation at steady state and power oscillation conditions to evaluate fuel rod thermal response, (b) power and cooling mismatch transients to evaluate boiling transition (BT) and return to nucleate boiling (RNB), and (c) RIA power excursions to measure fuel temperature distributions and help evaluate fuel failure limits. The fuel rod thermal response operation consisted of a two segment fuel rod power calibration, a preconditioning period, and a series of power oscillations. The boiling transition and RNB phase consisted of 23 coolant flow reductions and 2 power increase PCM transients. The RIA test phase included three power bursts at increasingly severe energy depositions.

2.2.1 Steady State and Power Oscillation Operation. The first segment of reactor power operation consisted of a series of rod power calibration steps to provide data to intercalibrate the test rod power with reactor power and thermal neutron flux. A heat balance of the system using the measured coolant flow rate, coolant temperature rise through the flow shroud, and coolant inlet temperature and pressure, was used to calculate rod power. The local power was determined using an axial power profile derived from previous PBF tests. The relationship between test rod power and neutron flux provided a method of determining test rod power when two phase exit conditions, such as

existed during the PCM transients, made an energy balance impractical. Data were also obtained to relate control rod position with test rod power, to assist in determining control rod positioning for the RIA power excursions.

The rod power calibration was performed by stepwise increasing and decreasing reactor core power (and thereby test rod power). An averaged test rod peak power of 46 kW/m was reached. Nominal coolant conditions during the first segment of the power calibration were: 6.45 MPa system pressure, 538 K inlet temperature, and 0.76 l/s volumetric flow rate through each flow shroud. The coolant conditions during the second segment of the power calibration were: 7.20 MPa system pressure, 540 K inlet temperature, and a shroud coolant flow rate adjusted between 0.20 and 0.60 l/s. The axial peak powers, volumetric flow rate through each flow shroud, and the coolant temperature rise at each power level of the power calibration and preconditioning phases are contained in Table 2. A schematic representation of the power calibration and preconditioning phases is provided in Figure 3.

A fuel rod preconditioning phase followed the first segment of power calibration. The purpose of the preconditioning was to allow fuel pellet cracking and restructuring. Steady state fuel rod thermal response data were obtained during the preconditioning phase to evaluate the effects of pellet cracking and fuel relocation on the fuel rod thermal response.

Nominal coolant conditions during preconditioning were: 540 K coolant inlet temperature, 7.17 MPa system pressure, and shroud coolant flow rates of about 0.20 and 0.40 l/s at averaged test rod peak powers of 13 and 28 kW/m, respectively.

Following the preconditioning period, a series of power oscillations was performed to evaluate the fuel-to-cladding gap conductance by the power oscillation method. Thermal response information was obtained by sinusoidally oscillating core power $\pm$ 20% at eight nominal power levels, and recording the relative phase lag between power and measured temperatures. At each power level the reactor was operated at steady state to assure equilibrium conditions prior to the oscillations, and to obtain steady state thermal response data. The oscillation conditions that were investigated are

TABLE 2. SUMMARY OF STEADY STATE THERMAL RESPONSE CONDITIONS

Reactor Core Power (MW)	Rod 524-1 Axial Peak Power (kW/m)	Rod 524-1 Shroud Coolant Flow Rate (l/s)	Rod 524-1 Coolant Temp. Rise (K)	Rod 524-2 Axial Peak Power (kW/m)	Rod 524-2 Shroud Coolant Flow Rate (l/s)	Rod 524-2 Coolant Temp. Rise (K)	Rod 524-3 Axial Peak Power (kW/m)	Rod 524-3 Shroud Coolant Flow Rate (l/s)	Rod 524-3 Coolant Temp. Rise (K)	Rod 524-4 Axial Peak Power (kW/m)	Rod 524-4 Shroud Coolant Flow Rate (l/s)	Rod 524-4 Coolant Temp. Rise (K)	Average Figure of Merit[c]
Power Calibration[a] (Segment 1)													
4.7	23.33	0.756	5.24	17.74	0.730	4.13	20.28	0.761	4.53	21.69	0.729	5.05	4.41
2.3	11.60	0.764	2.59	8.46	0.737	1.96	9.71	0.771	2.15	10.68	0.737	2.47	4.40
4.7	23.31	0.755	5.25	16.81	0.728	3.93	19.98	0.761	4.47	20.94	0.728	4.89	4.31
7.1	34.51	0.757	7.72	25.09	0.733	5.81	30.19	0.762	6.72	30.99	0.733	7.16	4.13
9.5	46.45	0.760	10.30	32.51	0.733	7.50	40.63	0.765	8.97	40.45	0.732	9.32	4.21
10.8	53.58	0.759	11.88	37.25	0.732	8.60	46.29	0.765	10.21	45.52	0.732	10.48	4.23
9.5	47.36	0.773	10.35	32.03	0.745	7.29	39.78	0.777	8.67	40.86	0.746	9.26	4.21
7.1	34.50	0.775	7.55	25.65	0.750	5.81	29.57	0.780	6.44	31.53	0.751	7.12	4.27
4.7	22.74	0.771	5.02	17.10	0.743	3.92	19.65	0.777	4.31	21.03	0.744	4.81	4.30
3.1	14.93	0.769	3.31	11.24	0.743	2.58	13.30	0.777	2.92	14.01	0.744	3.21	4.32
Power Calibration[b] (Segment 2)													
3.1	16.98	0.214	12.73	11.36	0.197	9.26	13.55	0.203	10.71	13.45	0.191	11.25	4.46
4.7	24.51	0.320	12.55	17.45	0.308	9.31	20.58	0.314	10.76	20.77	0.305	11.16	4.43
6.2	32.62	0.354	15.08	22.33	0.341	10.77	27.18	0.349	12.78	27.44	0.338	13.30	4.42
7.9	41.84	0.434	15.89	28.73	0.415	11.47	34.76	0.431	13.34	35.32	0.413	14.11	4.45
9.9	51.11	0.551	15.38	35.45	0.529	11.17	41.80	0.551	12.63	42.91	0.530	13.45	4.32
6.2	32.46	0.362	14.69	22.07	0.348	10.44	27.07	0.357	12.46	26.87	0.344	12.81	4.40
Preconditioning[b]													
3.1	15.44	0.173	14.30	10.51	0.163	10.34	11.88	0.163	11.66	13.13	0.156	13.40	4.11
6.2	33.30	0.366	14.91	21.98	0.347	10.43	27.29	0.360	12.46	25.80	0.344	12.31	4.37
3.0	16.52	0.183	14.35	11.08	0.169	10.45	12.86	0.173	11.79	12.84	0.161	12.58	4.40
6.2	32.54	0.419	12.83	22.28	0.398	9.27	26.71	0.414	10.68	26.68	0.397	11.12	4.36
3.0	16.41	0.180	14.43	11.03	0.166	10.55	12.69	0.170	11.83	12.72	0.158	12.66	4.40
6.2	32.26	0.412	12.93	22.12	0.392	9.35	26.43	0.407	10.75	26.66	0.390	11.30	4.33
3.0	16.34	0.183	14.17	10.97	0.169	10.35	12.36	0.173	11.37	12.64	0.162	12.37	4.36

a. Coolant inlet temperature of 538 K, system pressure of 6.45 MPa
b. Coolant inlet temperature of 540 K, system pressure of 7.20 MPa
c. Averaged rod power at the peak elevation divided by PBF Reactor Core Power

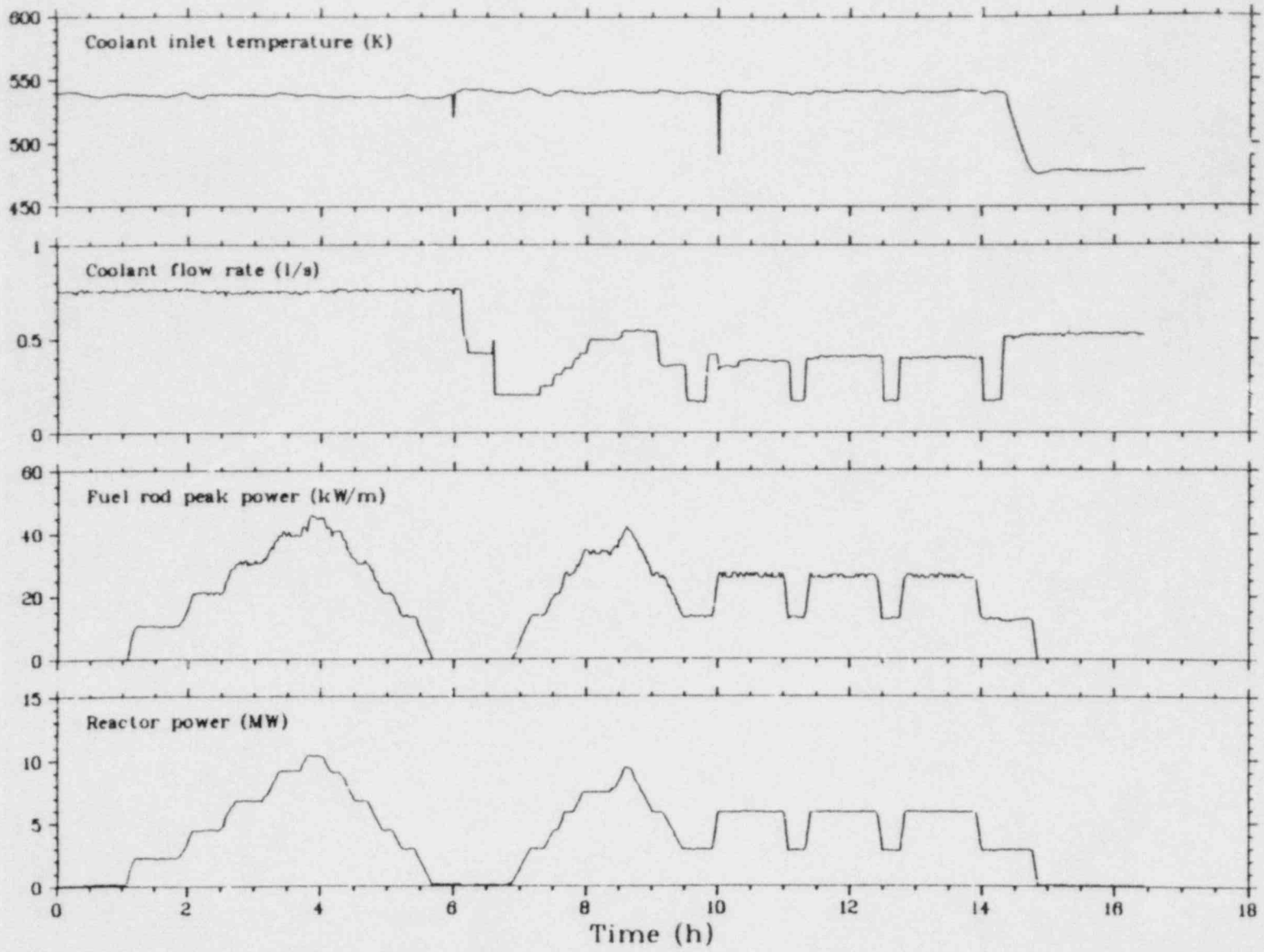

Figure 3. Test rod power, PBF core power and coolant conditions during Test PR-1 power calibration and preconditioning periods.

presented in Table 3. At each oscillation condition, the power was oscillated for approximately 40 cycles to obtain sufficient data to reduce statistical uncertainties. Coolant conditions during the power oscillation portion of the test were: inlet temperature of 478 K, system pressure of 7.17 MPa, and a coolant volumetric flow rate of about 0.52 l/s through each shroud.

2.2.2 PCM and Boiling Transition Transients. Twenty-three flow reduction and two power increase PCM transients were completed as a part of the boiling transition and return to nucleate boiling test phase. The objectives of performing these PCM transients were to evaluate the thermal-hydraulic conditions at onset of film boiling, to assess the potential for two-phase instabilities in the PBF 4-rod hardware geometry, and to evaluate the conditions at which return to nucleate boiling occurs.

Prior to the first PCM transient, a period of fuel rod aging was performed. This procedure was used to remove entrapped gases from the surface of the fuel rods and prevent premature boiling transition. The power-cooling-mismatch transients were conducted at approximate system pressures of 7, 13 and 15.5 MPa. The coolant temperature and flow conditions were consistent with those required to provide relatively constant inlet subcooling at each pressure condition.

Seven flow reduction transients were conducted at pressures between 7 and 8 MPa. The coolant inlet temperature was approximately 544 K for each transient. Eighteen PCM-type transients were conducted at system pressures between 13 and 15.5 MPa. The coolant inlet temperature at each pressure was adjusted to provide a nearly constant inlet subcooling (~ 14 K). Sixteen of the eighteen higher pressure transients were initiated by flow reduction at constant power, and two were initiated by increasing power at a constant coolant flow rate. Data were obtained during each transient to evaluate the potential for two phase instabilities in the PBF 4-rod hardware.

To evaluate the conditions at which return to nucleate boiling occured, various methods of inducing rewet were used. These methods included: (1) increasing flow and decreasing power simultaneously, (2) increasing flow rate at constant power, or (3) decreasing power at a constant flow rate. The

TABLE 3. POWER OSCILLATION CONDITIONS DURING TEST PR-1

Test Rod Peak Power (kW/m)	Oscillation Amplitude (±%)	Oscillation Period (s)	Rod Number to FRA[a] Input (Orientation)
11.84	20	20	524-1 (300°)
	20	20	524-3 (300°)
25.02	20	20	524-1 (60°)
	20	20	524-4 (140°)
37.44	20	20	524-1 (60°)
	20	20	524-3 (300°)
50.52	20	20	524-1 (60°)
	20	20	524-4 (140°)
Repeats:			
11.84	20	20	524-1 (60°)
	20	20	524-4 (140°)
24.94	20	20	524-1 (60°)
	20	20	524-3 (300°)
37.11	20	20	524-1 (60°)
	20	20	524-4 (140°)
51.77	20	20	524-1 (60°)
	20	20	524-3 (300°)

a. The FRA is a frequency response analyzer which computes the phase lag between the driving signal (power) and response signal (cladding surface temperature measurement). The rod number and orientation refer to a cladding thermocouple orientation on the specified test rod (all at 0.452-m elevation).

PBF core power, peak test rod power, coolant inlet temperature, system pressure, and transient description corresponding to each transient are listed in Table 4.

2.2.3 Power Burst Test Conduct. The power burst phase of Test PR-1 consisted of three power bursts. A brief steady-state power calibration preceded each power burst to ensure that the figure-of-merit (ratio of test rod power to reactor power) had not significantly changed as a result of the previous testing. New, 100% cobalt flux wires were installed in the reactor prior to each power burst. The neutron fluence measured from the flux wire activations together with posttest radiochemical fission product analyses will provide final power burst fuel energy data. The coolant conditions for each power burst were nominally 538 K inlet temperature, 6.45 MPa system pressure, and 0.109 l/s coolant volumetric flow rate, which are representative of BWR hot startup conditions.

A reactivity balance was conducted prior to initiation of each power burst. This balance provided assurance that the control and transient rods had not been grossly malpositioned, and no potentially dangerous reactivity addition could be made. The procedure to initiate each power burst is detailed below.

1. The control rods were withdrawn from their scram positions until a reactor transient period of about 10 s was achieved. The reactor power was then increased until two reactor console panel lights indicated the plant protection system was operating correctly. Immediately following verification that the plant protection system was operating, the control rods were inserted until the reactor was subcritical.

2. The control rods were then slowly withdrawn until criticality was achieved at a power of about 100 W, and the low power critical position of the control rods determined.

3. The transient rods were inserted into the core to a calculated position worth a negative reactivity equivalent to the reactivity insertion required for each power burst.

TABLE 4. POWER-COOLING-MISMATCH TRANSIENT CONDITIONS

	PBF Core Power (MW)	Test Rod Peak Power (kW/m)	Coolant Inlet Temperature (K)	System Pressure (MPa)	Transient Description
1.	10.1	40.39	545	7.2	Flow reduction at constant test rod power
2.	11.4	43.19	543	7.3	Flow reduction at constant test rod power
3.	12.5	47.21	548	7.3	Flow reduction at constant test rod power
4.	12.5	49.18	545	7.2	Flow reduction at constant test rod power
5.	12.5	49.59	547	7.3	Flow reduction at constant test rod power
6.	12.5	47.42	550	7.2	Flow reduction at constant test rod power
7.	12.7	43.71	594	12.7	Flow reduction at constant test rod power-transient concluded by simultaneous flow increase and power reduction
8.	11.8	42.12	607	15.5	Flow reduction at constant test rod power-transient concluded by simultaneous flow increase and power reduction
9.	11.8	42.12	610	15.5	Flow reduction at constant test rod power-transient concluded by simultaneous flow increase and power reduction
10.	11.1	42.12	595	13.4	Flow reduction at constant test rod power
11.	11.1	40.95	594	13.0	Flow reduction at constant test rod power
12.	12.2	45.67	595	13.2	Flow reduction at constant test rod power-transient concluded by simultaneous flow increase and power reduction
13.	12.5	48.86	553	7.3	Flow reduction at constant test rod power
14.	12.5	46.92	593	13.0	Flow reduction at constant test rod power-transient concluded by simultaneous flow increase and power reduction
15.	12.5	44.83	593	13.1	Flow reduction at constant test rod power-transient concluded by increasing flow
16.	11.8	41.63	603	15.5	Flow reduction at constant test rod power-transient concluded by increasing flow
17.	11.8	40.87	604	15.6	Flow reduction at constant test rod power-transient concluded by increasing flow
18.	12.5	45.50	593	12.9	Flow reduction at constant test rod power-transient concluded by increasing flow
19.	12.5	45.50	593	12.9	Flow reduction at constant test rod power-transient concluded by increasing flow
20.	12.5	45.50	593	12.9	Flow reduction at constant test rod power-transient concluded by increasing flow
21.	11.8	42.41	606	15.4	Flow reduction at constant test rod power-transient concluded by increasing flow
22.	12.6	46.53	575	15.0	Flow reduction at constant test rod power-transient concluded by increasing flow
23.	12.6	42.24	605	15.2	Flow reduction at constant test rod power-transient concluded by increasing flow
24.	6-12.7	25.00-44.94	590	15.6	Power increase at constant flow rate-transient concluded by power decrease
25.	6.5-15.3	22.44-53.70	590	15.5	Power increase at constant flow rate-transient concluded by power decrease

4. The control rods were then adjusted to the withdrawal position corresponding to the calculated increment for the desired reactivity insertion. The control rod withdrawal increment was checked with the transient rod insertion increment to ensure that a gross error in the control rod increment had not been made.

5. The transient rods were fully inserted into the core, leaving the control rods in a position corresponding to a calculated reactivity increment (above low-power critical) that was equivalent to the reactivity insertion desired.

6. The power burst was initiated by ejecting the four transient rods at a velocity of about 9.5 m/s. The burst was self-terminating because of the inherent Doppler reactivity feedback in the PBF. The feedback is capable of terminating power bursts without primary dependence on mechanical systems.

7. All eight control rods were then completely inserted into the driver core to provide mechanical shutdown of the reactor.

3. FUEL ROD THERMAL RESPONSE DURING TEST PR-1

Thermal response data were obtained from Test PR-1 to complement similar data from previous Gap Conductance (GC) Test Series[1] experiments. Since the Test PR-1 hardware was originally designed for a Gap Conductance Series experiment, instrumentation were optimally positioned for these measurements.

Data were obtained during the power calibration, preconditioning, and power oscillation test segments from which the fuel rod thermal behavior could be deduced and compared to previous GC results. Response data from the repeated boiling transition transients is complicated by fuel rod dimensional changes, fuel restructuring, and cladding oxidation. Interpretation of these data will be deferred for subsequent analysis. This section presents the Test PR-1 preliminary steady state and power oscillation response data, and a comparison with applicable data from prior experiments.

3.1 Steady State Fuel Rod Thermal Response

Analysis of data from Test PR-1 will ultimately provide interpretation of fuel rod stored energy, gap conductance, effective fuel conductivity, and pellet cracking (and relocation) in boiling water reactor type fuel rods. These analyses require qualified data with effects such as thermocouple perturbations and uncertainties included. The raw data, however, provide thermal response trends relative to the fuel rod design parameters. The data of primary interest include fuel centerline temperatures, off-center fuel temperatures, and cladding surface temperatures in conjunction with fuel rod local power. The design parameters of interest for Test PR-1 include fuel density (Rods 524-1, 524-2, and 524-3 were identical except for fuel densities of 95, 92, and 97% of theoretical, respectively) and fill gas composition (Rods 524-3 and 524-4 were identical except for fill gas compositions of helium and argon, respectively). Power levels at which steady state response data were obtained during Test PR-1 are listed in Table 5. Preliminary steady state gap conductance values determined by the $\int k dT$ method[1] are also shown on Table 5. The values shown were obtained using both centerline and off-center fuel temperature measurements in conjunction with averaged cladding surface temperature measurements.

TABLE 5. STEADY STATE CALCULATED GAP CONDUCTANCE VALUES USING ∫kdT METHOD

Averaged Test Rod Peak Power (kW/m)	Gap Conductance[a] ($kW/m^2 \cdot K$)				Gap Conductance[b] ($kW/m^2 \cdot K$)			
	Rod 524-1	Rod 524-2	Rod 524-3	Rod 524-4	Rod 524-1	Rod 524-2	Rod 524-3	Rod 524-4
20.76	2.92	3.46	2.72	1.09	4.28	4.49	3.21	1.68
10.11	2.23	2.51	2.14	0.63	3.08	2.90	2.49	0.82
20.26	--	3.20	2.75	1.01	4.37	4.11	3.20	1.65
30.20	3.84	4.75	3.65	1.51	5.98	6.74	4.65	3.08
40.01	5.18	6.79	4.80	2.12	8.59	11.05	6.41	4.45
45.66	6.17	8.08	5.52	2.48	11.22	14.26	7.58	5.19
40.01	4.89	6.27	4.48	1.89	7.19	7.81	6.23	3.40
30.31	3.84	4.70	--	--	4.22	4.91	--	--
20.13	2.92	3.41	2.76	0.93	3.17	3.63	3.15	5.24[c]
13.37	2.50	2.97	2.41	0.73	2.70	3.17	2.68	2.38[c]
13.84	2.78	3.44	2.67	0.86	2.93	3.48	2.92	2.67
20.83	3.22	--	3.06	1.12	3.46	4.02	3.47	1.80
27.39	3.98	5.08	3.71	1.40	4.30	4.54	4.33	2.84
35.16	5.12	6.62	4.74	1.80	5.91	6.68	5.96	4.53
42.82	6.07	8.01	5.56	2.22	10.01	11.37	7.26	7.48
27.12	3.92	4.85	3.73	1.30	4.18	4.98	4.29	6.61
12.74	2.49	3.09	1.88	0.78	2.69	3.31	2.69	2.38
27.09	3.91	4.80	3.82	1.37	4.26	4.90	4.38	5.24[c]
13.33	2.76	3.43	2.79	0.82	2.84	3.67	3.05	3.78
27.05	3.93	4.87	3.86	1.37	4.24	5.02	4.27	5.35[c]
13.21	2.74	3.42	2.78	0.83	2.85	3.60	3.08	3.27[c]
26.87	3.85	4.80	3.81	1.35	4.19	4.96	4.27	5.45[c]
13.08	2.73	3.43	2.78	0.82	2.83	3.65	3.08	3.14[c]

a. Gap conductance values calculated using ∫kdT method with measured fuel centerline and cladding surface temperatures.
b. Gap conductance values calculated using ∫kdT method with azimuthally averaged off-center fuel and cladding surface temperature measurements. Off-center temperature measurements not corrected for thermocouple perturbation effects.
c. Values based on single off-center measurement due to failure of other devices.

Test rod local power was determined from a calorimetric heat balance of each test rod, and an axial power distribution from previous experiments[a]. The heat balance was accomplished using measured coolant conditions (pressure and inlet temperature), shroud volumetric flow rate, and coolant temperature rise through each shroud. Subcooled inlet and outlet conditions were maintained at all power levels to ensure accurate coolant enthalpy determination. The first segment of the power calibration was conducted at a high coolant flow rate to ensure subcooled forced convection heat transfer over the entire test rod. During the second segment of the power calibration, the coolant flow rate was adjusted to preclude bulk outlet saturation, but allow high cladding surface heat transfer at the primary measurement (peak power) axial elevation.

The average linear heat generation of each test rod, determined from the energy balance, was adjusted to a local power generation by applying a peaking factor of 1.35. Differences in measured linear power between the four rods were attributed to measurement uncertainties rather than inherent differences in test rod power generation, and hence were averaged to obtain the values of Table 5.

Fuel centerline temperatures as a function of test rod peak power (averaged) is shown in Figure 4 for the three helium filled rods with variations in fuel density. As was seen in previous experiments, the effect of fuel density variations between 92 and 97% of theoretical, is minimal. The minor variations noted are well within expected uncertainties in the measured centerline temperatures. Similar results were obtained by comparing the measured off-center temperatures for Rods 524-1, 524-2 and 523-3. Azimuthal variations in measured off-center fuel temperatures outweighed any difference in temperature due to fuel density variation.

---

a. The axial power profile for Test PR-1 was determined from flux wire scans of previous tests at the same experiment coolant conditions. The PBF core flux shape generally governs the axial profile and is not significantly effected by the experiment conditions.

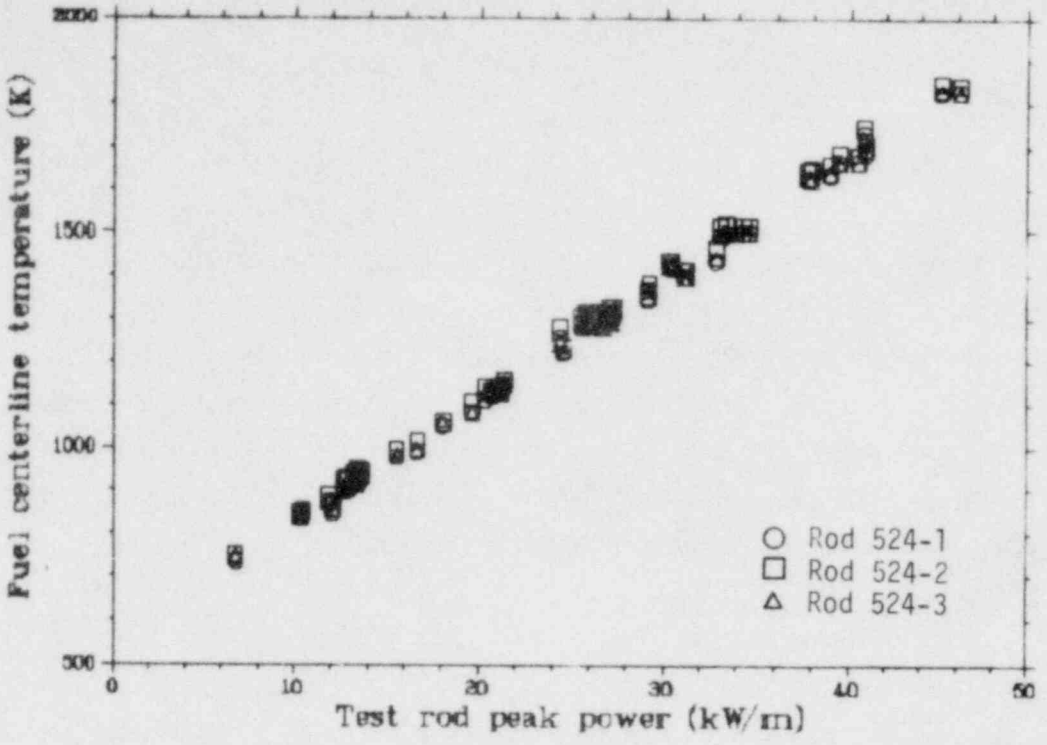

Figure 4. Measured centerline temperatures as a function of test rod power for the Test PR-1 helium filled rods with variations in fuel density.

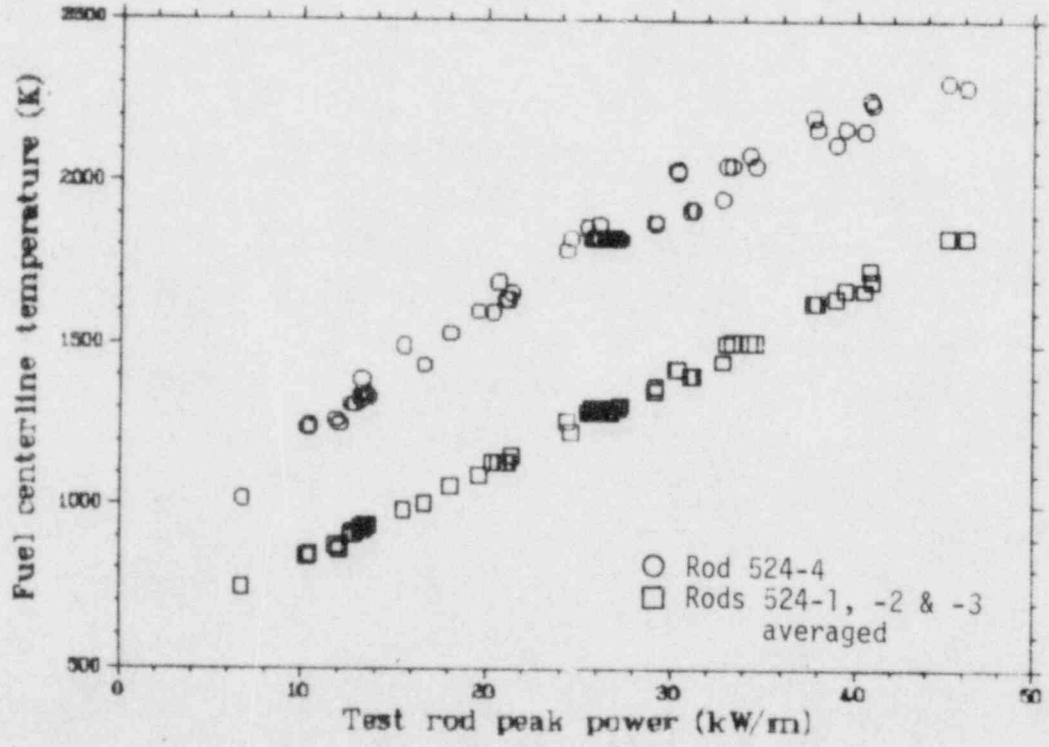

Figure 5. Measured centerline fuel temperatures showing the effect of fill gas composition between helium and argon filled test rods.

The effect of fill gas composition under steady state conditions is illustrated in Figure 5. Shown is the measured fuel centerline temperature (as a function of test rod power) for a helium filled rod (524-3) and the argon filled rod (524-4) with other design features common. The gas conductivity in the argon filled test rod results in a higher fuel centerline temperature at each power level considered. Fuel centerline temperatures in the argon filled rod were consistently 400 to 500 K higher than the helium rod temperatures at test rod powers above 13 kW/m.

Comparison between measured and predicted fuel centerline and off-center temperatures for two different fuel models (Coleman relocation and free thermal expansion) is shown in Figure 6. The predictions[2] were conducted using the FRAP-T[a] computer code for the Test PR-1 helium filled rods. The Ross and Stoute (modified) gap conductance model was used in conjunction with the two fuel models. Shown for reference is the predicted gap conductance using the two fuel models. In general, the prediction using the free thermal expansion fuel model agrees well with the trend and magnitude of the centerline temperature data in the helium filled test rods. Calculated off-center fuel temperatures using the Coleman relocation fuel model agree well with the measured off-center fuel temperatures.[b]

A similar comparison between measured and predicted temperatures in the argon filled test rod (Rod 524-4, are shown in Figure 7. The free thermal expansion fuel model slightly overpredicts the argon rod centerline fuel temperatures, whereas the Coleman relocation fuel model underpredicts the same temperatures by a larger magnitude. Only measured off-center fuel temperature data from the first power increase is shown for the argon filled test rod due to subsequent deterioration of these measurement devices. The Coleman relocation model appears to approximate the off-center temperature data better than the free expansion model, although neither appears generally consistent with the limited data available.

---

a. FRAP-T5, Idaho National Engineering Laboratory Configuration Control Number H0005838.
b. Azimuthal variations in measured off-center fuel temperature were neglected in this comparison by averaging the off-center temperature measurements.

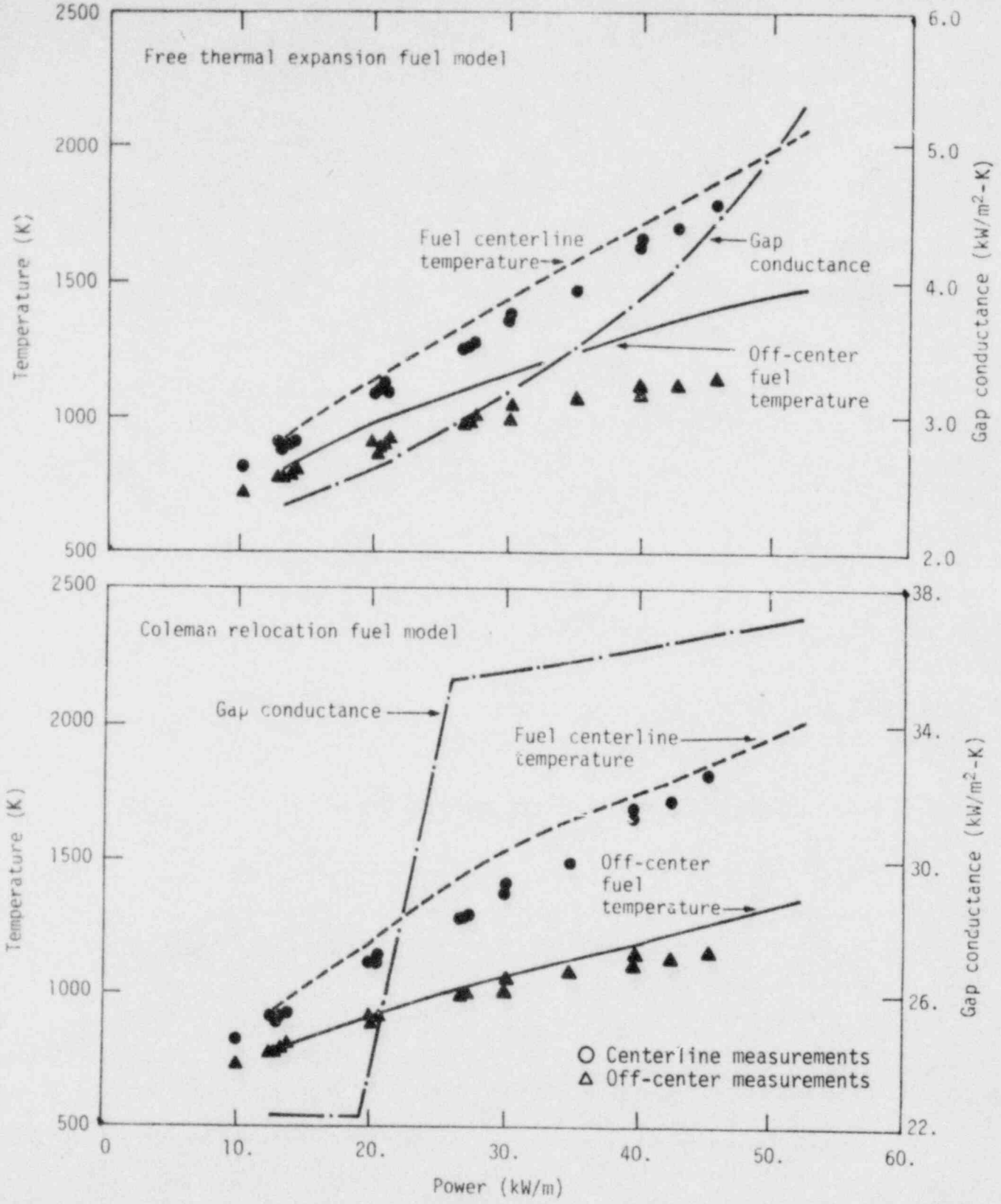

Figure 6. Comparison of measured and predicted centerline and off-center fuel temperatures for the Test PR-1 helium filled rods using two fuel models.

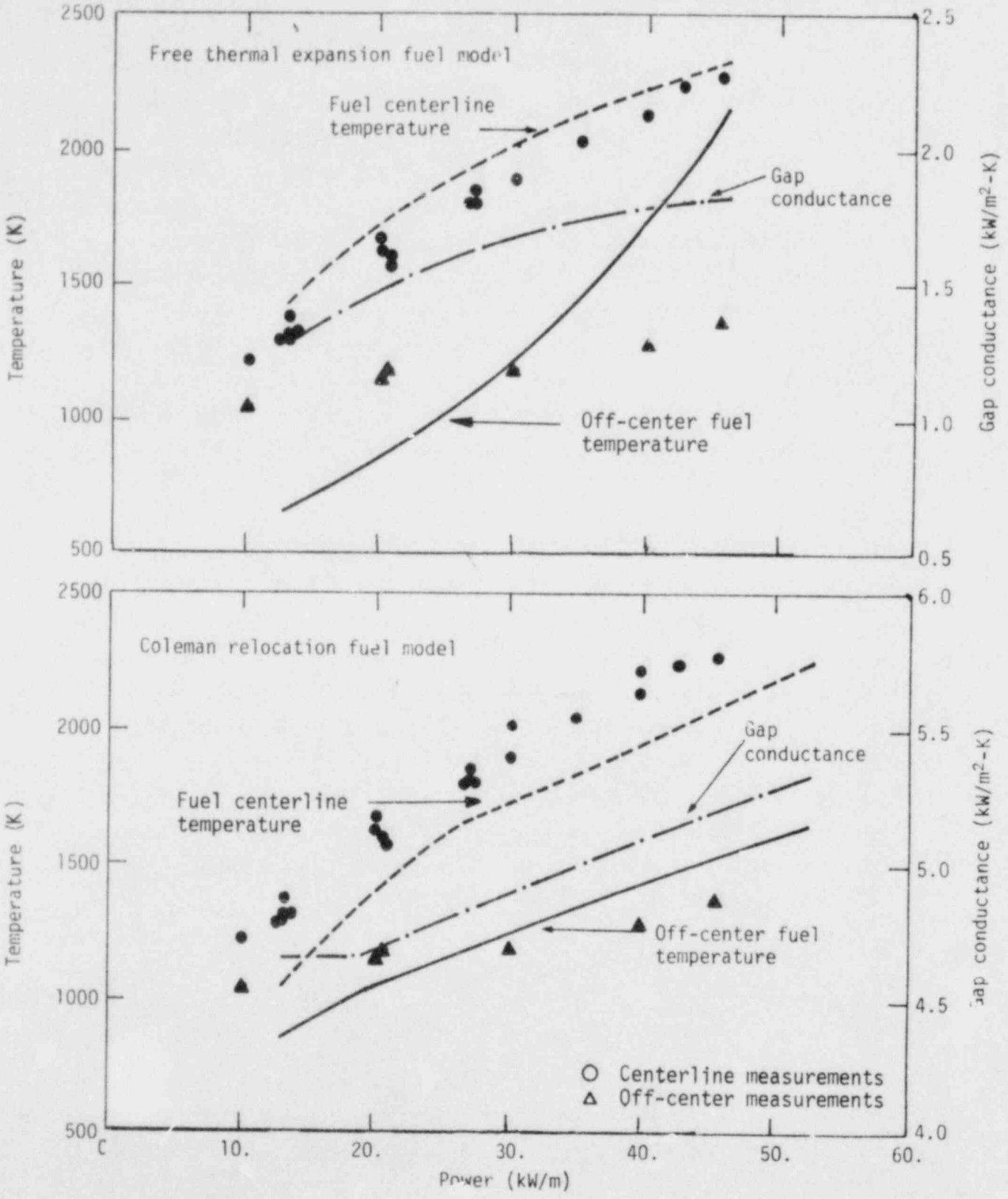

Figure 7. Comparison of measured and predicted centerline and off-center fuel temperatures for the Test PR-1 argon filled test rod using two fuel models.

3.2 Fuel Rod Response During Power Oscillations

The power oscillation or thermal oscillator method of determining fuel rod response parameters relates a sinusoidal driving function (power) to the resulting phase lag in various fuel rod response parameters. Inherent in the method is the assumption that the fuel rod response is a linear function of the driving function; i.e., that changes in fuel conductivity, gap conductance, etc. are sufficiently small during the oscillation that measured temperatures are proportional to the driving function with some measurable phase lag between the signals. The primary usefulness of the power oscillation technique (if it proves reliable) would be to infer gap conductance on irradiated fuel rods from only the external surface (cladding) temperature response to a driving function. Data were obtained during Test PR-1 to help evaluate the thermal oscillator method and the modeling assumptions associated with the technique.

The phase lag between cladding temperature and power were used to evaluate gap conductance by the oscillation method during Test PR-1. Data were obtained at four power levels with repeat data obtained at each level. The nominal oscillation power levels, measured phase angles between power and cladding temperature, and associated gap conductance values are shown in Table 6. Gap conductance values were deduced from the measured phase angles using a series of curves generated by the HEAT-1[a] computer code. A range of gap conductance values and the specific oscillation conditions were input to the code and the resulting phase angle relationships evaluated. Highly subcooled conditions were maintained at the measurement elevation (0.452 m) during the power oscillations to minimize the perturbation effects on measured cladding temperature due to nucleate boiling. The coolant conditions were: inlet temperature of 478 K, system pressure of 7.17 MPa, and nominal coolant flow rate through each shroud of 0.2 l/s (2700 $kg/m^2 \cdot s$ mass flux).

Also shown on Table 6 are steady state gap conductance values (by the $\int kdT$ method) obtained prior to each power oscillation condition. Comparison of the gap conductance values obtained by the power oscillation method with

---

a. HEAT-1 Idaho National Engineering Laboratory Configuration Control Number HO12582B.

TABLE 6. POWER OSCILLATION TEST RESULTS AND COMPARISON WITH STEADY STATE GAP CONDUCTANCES

Test Rod[a] Peak Power (kW/m)	Test Rod (Orientation)	Measured Phase Angle (Deg)	95% Uncert. In Measured Phase Angle (± Deg)	Gap Conductance From Measured Phase Angle ($kW/m^2 \cdot K$)	Gap Conductance[b] From $\int kdT$ Method ($kW/m^2 \cdot K$)
11.84	524-1 (300°)	48.68	1.09	5.45	2.20
11.84	524-3 (300°)	52.59	0.71	4.17	2.34
25.02	524-1 (60°)	45.36	0.31	8.97	2.91
25.02	524-4 (140°)	48.98	0.60	5.61	1.26
37.44	524-1 (60°)	44.04	0.34	10.82	3.97
37.44	524-3 (300°)	44.64	0.45	9.68	4.07
50.52	524-1 (60°)	40.57	0.46	21.49	5.58
50.52	524-4 (140°)	35.63	0.33	57.53	3.06
11.85	524-1 (60°)	47.10	0.46	6.40	2.45
11.85	524-4 (140°)	66.56	0.83	1.20	0.76
24.94	524-1 (60°)	46.65	0.38	7.50	3.15
24.94	524-3 (300°)	47.36	0.31	6.83	4.79
37.11	524-1 (60°)	43.05	0.33	13.39	4.28
37.11	524-4 (140°)	37.74	0.46	68.21	1.70
51.77	524-1 (60°)	41.09	0.34	17.73	6.50
51.77	524-3 (300°)	37.85	0.60	63.45	9.86

a. All power oscillations were conducted at ± 20% of nominal power level and a period of 20 s/cycle. All oscillations were conducted at an inlet temperature of 478 K and system pressure of 7.17 MPa.
b. Steady state ($\int kdT$) gap conductance calculated using appropriate centerline and cladding temperature measurements.

those obtained by the generally accepted $\int kdT$ method, reveal large discrepancies in the values obtained by the two methods. Apparently, nonlinear changes in the fuel rod parameters or intermittent pellet-to-cladding contact during the power oscillations are effecting the phase angle vs gap conductance relationships. Waveform analysis of prior power oscillation data suggest that nonlinearities in the response measurement (cladding temperature) are more pronounced in BWR-type fuel rods than PWR-type rods[1]. The speculated cause of the difference between fuel rod types was enhanced pellet and cladding contact in the BWR flat end pellet design during power oscillations. Continued analysis of the Test PR-1 oscillation data in conjunction with previously obtained data may provide more insight into these effects as well as helping to interpret the complex mechanisms involved in fuel rod thermal response under transient conditions.

3.3 Comparison of Thermal Response Data from Test PR-1 with GC Test Series

The Test PR-1 steady state thermal response data can be directly compared to data obtained in the Gap Conductance Test Series since the Test PR-1 fuel rods were of similar design, and had design parameter variations supporting the GC test matrix. All fuel rods in Test PR-1 had nominal diametral gaps of 0.22 mm (2.2% of initial fuel pellet diameter) to provide direct comparative data. The effect of fill gas composition on fuel centerline temperatures is shown in Figure 8. A similar comparison with off-center fuel temperatures is seen in Figure 9. The trend data from Test PR-1 are in good agreement with steady state results from other testing on common gap fuel rods.[a]

The effect of initial gap width upon fuel centerline temperatures for helium and argon filled test rods are shown in Figures 10 and 11. The 2.2% gap data from Test PR-1 are generally consistent with previous data although the temperature trends are slightly lower. These trends will be further evaluated using the qualified data from Test PR-1.

---

a. Test rod powers for Rods 524-2 and 524-3 were increased by 1 and 2 kW/m, respectively, for graphical clarity on Figures 8, 9 and 10.

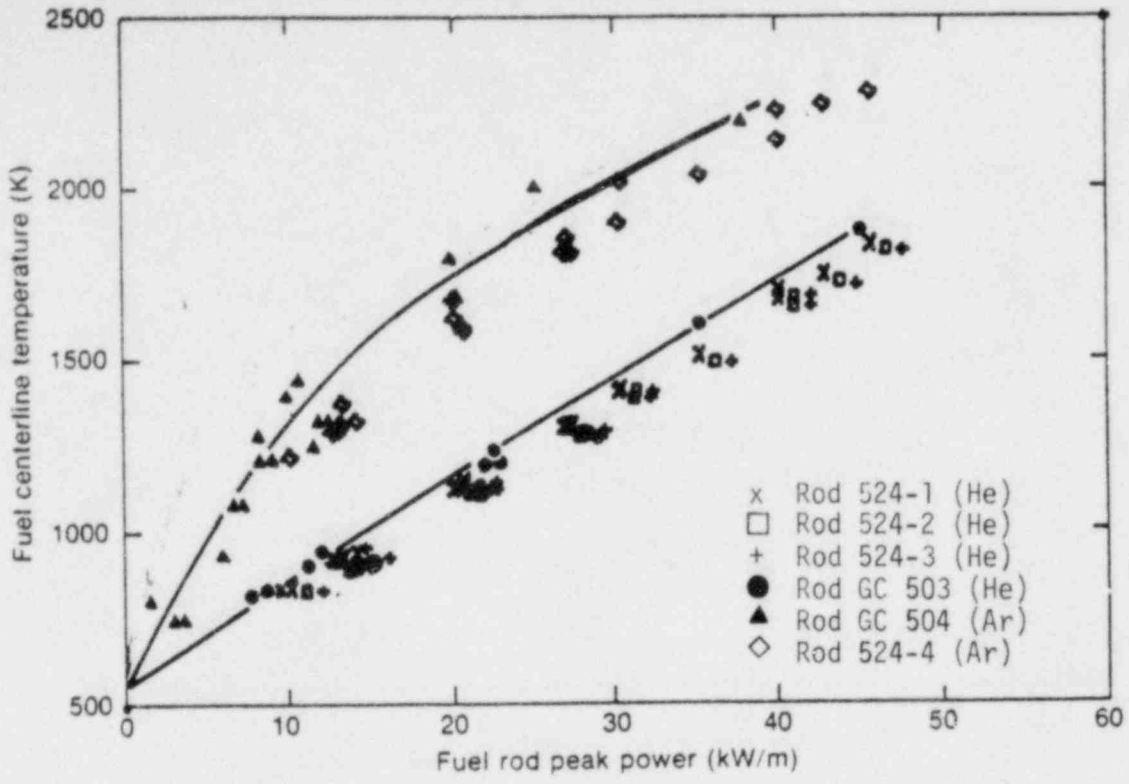

Figure 8. Comparison of Test PR-1 centerline temperature measurements with previous GC experimental data showing the effect of fill gas composition.

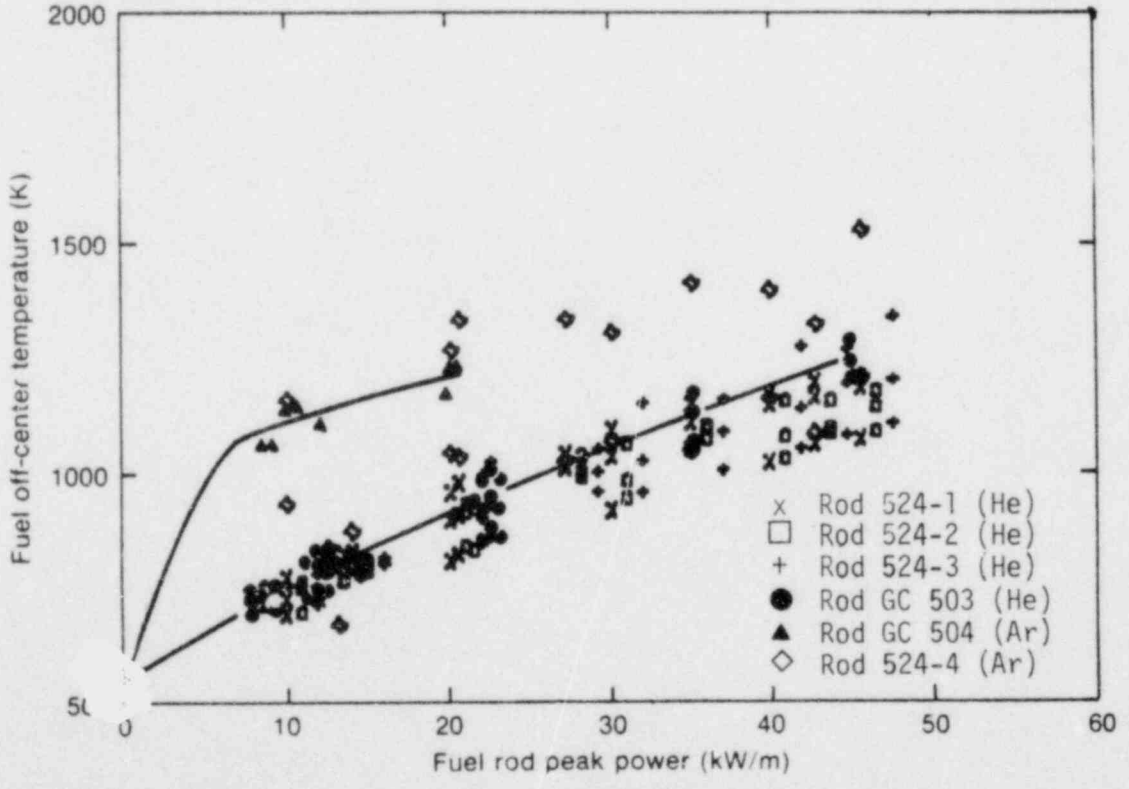

Figure 9. Comparison of Test PR-1 off-center fuel temperature measurements with previous GC experimental data showing the effect of fill gas composition.

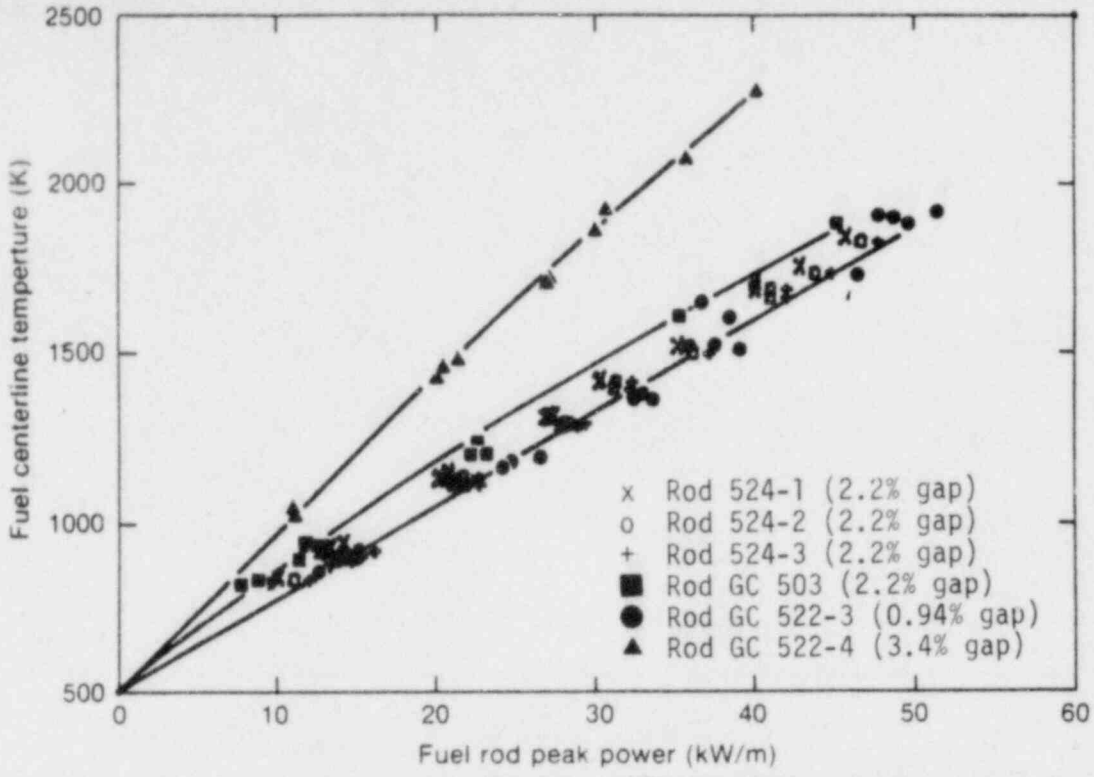

Figure 10. Test PR-1 centerline temperature measurements compared with prior GC experiment results showing the effect of initial gap width in helium filled test rods.

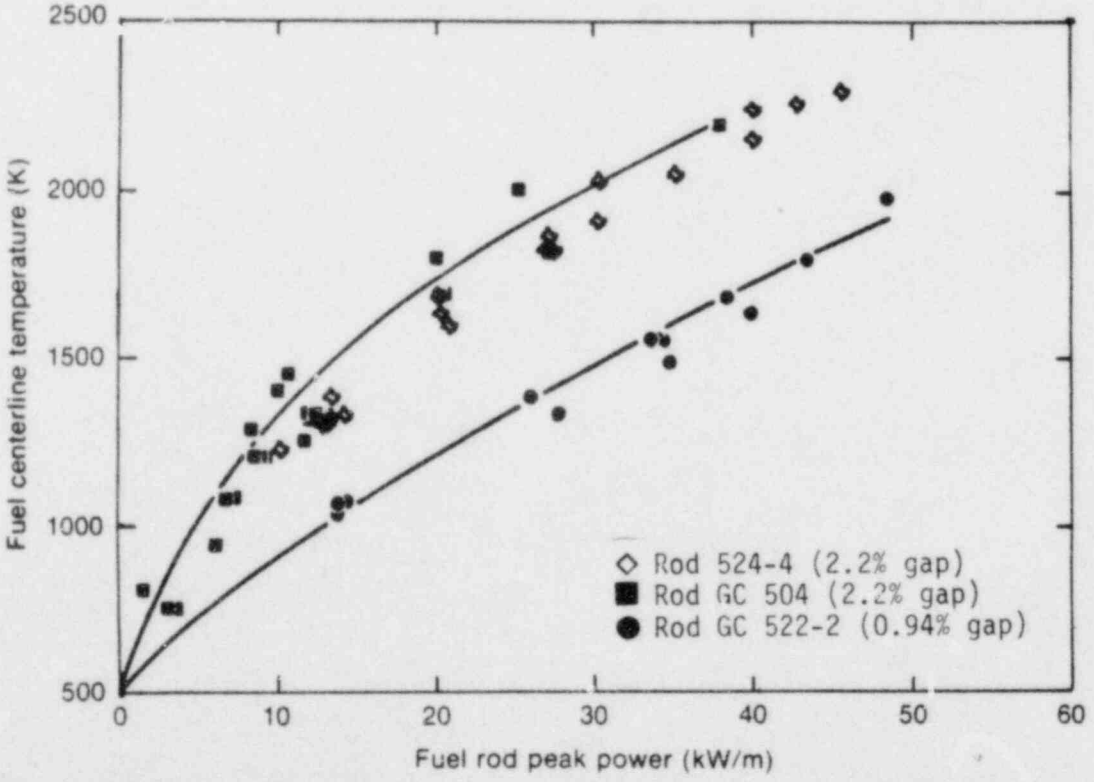

Figure 11. Test PR-1 centerline fuel temperature measurements compared with prior GC experiment results showing the effect of initial gap width in argon filled test rods.

4. PCM AND BOILING TRANSITION RESULTS

Specific objectives of Test PR-1 included providing information on boiling transition, return to nucleate boiling, and the potential for two-phase hydrodynamic instabilities in the PBF 4-rod hardware. A series of 23 flow reductions (at constant power) and 2 power increase transients (at constant flow) were conducted to attain these objectives. Boiling transition was observed during at least 13 of the transients, all at the higher system pressures considered (13.0 and 15.5 MPa). Within this section, a general (Quick Look) comparison between high and low pressure boiling transition, and natural circulation considerations as related to Test PR-1 are presented. Preliminary results and observations regarding boiling transition, return to nucleate boiling, and the potential for two-phase instabilites during Test PR-1 are also presented.

4.1 General Phenomena Associated With Boiling Transition

The consequences of boiling transition in a light water reactor environment can range from slight to severe depending on the dominant heat transfer processes and the mitigating actions taken. Test PR-1 was conducted, in part, to provide information on boiling transition and return to nucleate boiling under a variety of coolant conditions representative of the heat transfer modes which might be expected in an LWR under postulated accident conditions. Within this section, a general, "Quick Look" interpretation of the boiling transition phenomena for the Test PR-1 operating conditions is presented.

4.1.1 Comparison of Boiling Transition Under PWR and BWR Conditions.

The phenomena and consequences of boiling transition in a PWR environment may be significantly different from that experienced in a BWR environment. Such differences can readily be seen by comparing the respective forced convection "boiling curves". A simplified illustration of the forced convective boiling curves considered representative for high (PWR) and low (BWR) pressure conditions is shown in Figure 12. For the high pressure condition, (Figure 12-A), more indicative of a PWR-type environment, different heat transfer regimes are progressively seen as heat flux increases. As the

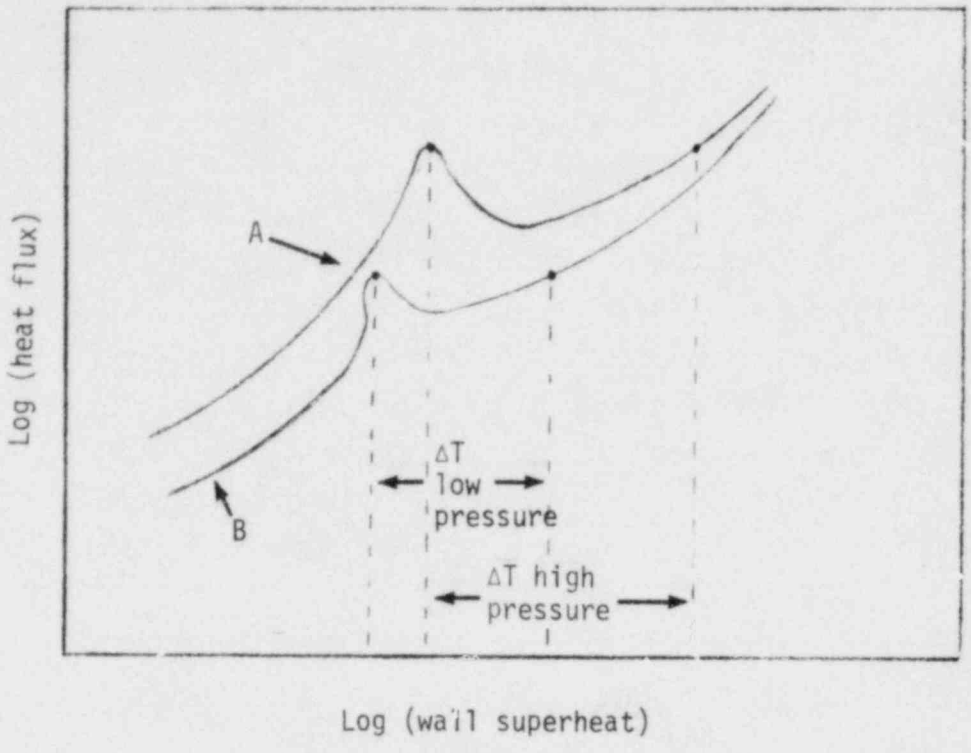

Figure 12. Representative forced convection boiling curves for high and low pressure conditions.

surface heat flux increases to the boiling transition[a] the primary heat transfer mechanism progresses from subcooled forced convection to a partial boiling and subcooled nucleate boiling regime. For a heat flux controlled system, boiling transition results in a large decrease in the heat transfer coefficient (due to estabishment of an insulating vapor film) and a corresponding large increase in wall temperature. This transition is commonly referred to as subcooled departure from nucleate boiling (DNB) and results in high temperature, film boiling operation. Most transients in the Power-Cooling-Mismatch Test Series and the higher pressure transients of Test PR-1 were conducted under PWR-type conditions, and are generally described by such a boiling transition scenario.

The low pressure (BWR pressures) transients of Test PR-1 are generally described by a forced convection boiling curve as illustrated in Figure 12-B. At lower heat fluxes, the primary heat transfer regimes include two-phase forced convection and saturated nucleate boiling. Just prior to boiling transition (as the surface heat flux increases), an additional mechanism of heat transfer may be encountered for high quality annular flows, such as may occur in BWR technology. In this mode, the vapor velocity and interfacial turbulence level can become so high, and the liquid film so thin, that nucleation is suppressed on the heated surface. This regime, known as forced convective vaporization, results in high heat transfer coefficients and, thus, as the heat flux is increased, the wall temperature may decrease. At the boiling transition, the heat transfer decreases and the wall temperature increases. The magnitude of the wall temperature increase is a function of the quality at which boiling transition occurs and, in general, is less than for a subcooled DNB excursion.

The effect of quality on the wall temperature excursion, based on the work of Plummer et al.,[3] is illustrated in Figure 13 for two different coolant mass fluxes. As the equilibrium quality at boiling transition

---

a. The literature refers to boiling transition by several descriptive terminologies, depending on the reference environment. Some of these include (1) Critical Heat Flux (CHF), (2) Departure from Nucleate Boiling (DNB), (3) Boiling crises, (4) Dryout and (5) Burnout heat flux. The terminology used within this report is "boiling transition" since the interchange of names becomes confusing over the range of Test PR-1 operating conditions.

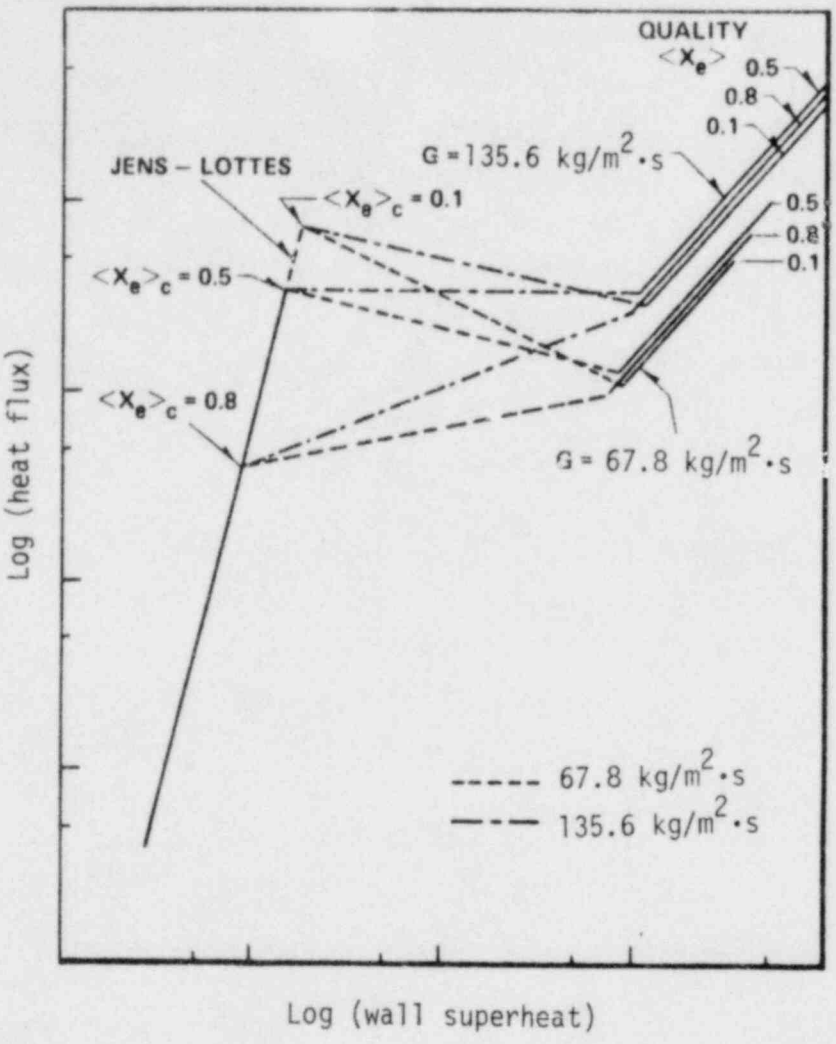

Figure 13. Boiling curves for water showing effect of Quality on Boiling Transition (Plummer et al., 1974).

($\langle Xe \rangle_c$ on Figure 13) decreases, the boiling transition heat flux and the corresponding wall thermal excursion increases. For the high quality condition ($\langle Xe \rangle_c = 0.8$) the unstable, negative slope transition boiling region is not evident. This suggests that operation in this region may be accomplished with minimal wall temperature excursions. The low pressure (~7 MPa) flow reductions of Test PR-1 did not result in readily detectable boiling transitions. Either the rods did not attain boiling transition, or the boiling transition resulted in very low wall temperature excursions, not detectable by the test train instrumentation. The expected quality at onset of boiling transition was near 0.8 at the low pressure condition, suggesting that the latter explanation for not detecting boiling transition is plausible.

4.1.2 Natural Circulation Considerations during Test PR-1. Several attempts were made during Test PR-1 to reduce flow sufficiently to induce boiling transition at the low pressure conditions. Various combinations of IPT bypass and flow control valve settings (see Figure 2) were tried in order to influence the flow reduction capability. With all combinations, the minimum measured flow rate through the individual coolant shrouds was limited (at power) to values between 0.07 and 0.08 l/s. With no test rod power generation, the coolant flow rate could be reduced to nearly 0.03 l/s. It is expected that natural circulation limited the flow reduction. The low flow limitation was observed at all pressure levels and test rod powers between 40 and 53 kW/m. A quantitative explanation of the low flow limitation for the Test PR-1 geometry follows.

The coolant within the in-pile bypass region was subcooled during the entire Test PR-1 operation. In contrast, saturated or boiling conditions existed within the individual coolant flow shrouds during power operation. Therefore, during power operation, the coolant density within the in-pile bypass (ρ_{BP}) was greater than the average flow shroud coolant density (ρ_{FS}). As a result of this density differential, a driving pressure (ΔP_d) is established, and is given by

$$\Delta P_d = \begin{pmatrix}\text{Hydrostatic pressure} \\ \text{within in-pile bypass}\end{pmatrix} - \begin{pmatrix}\text{Hydrostatic pressure} \\ \text{within coolant flow shroud}\end{pmatrix} \qquad (1)$$

$$= \left(\rho_{BP} H_{BP} - \bar{\rho}_{FS} H_{FS}\right) g$$

where H_{BP} and H_{FS} are the vertical lengths of the bypass and flow shroud, respectively. In addition to the free or natural convection contribution to the driving pressure (Equation 1), the PBF pump also supplied a driving pressure (ΔP_p) which resulted in a zero power volumetric flow rate of about 0.03 l/s. The total driving pressure, therefore, is given by

$$\Delta P_T = \Delta P_d + \Delta P_p \tag{2}$$

At a given coolant flow rate (G) the total driving pressure (Equation 2) must equal the total system pressure losses (ΔP_S) which, for a flowing two-phase system, are given by

$$\Delta P_S = \Delta P_f + \Delta P_a + \Delta P_g \tag{3}$$

where the subscripts f, a, and g refer to friction, acceleration, and gravity pressure drops, respectively.

Theoretically, if all driving pressures (Equation 2) and all pressure loss terms (Equation 3) are known, the resultant coolant flow rate (G) may be calculated. Unfortunately, several of the pressure terms are functions of coolant flow rate (G) and, thus, an iterative-type solution is required. Such a solution is beyond the scope of this report, however, an alternate method of esimating the coolant flow rate follows.

The alternate method of estimating the total volumetric coolant flow rate within an individual coolant shroud is based on the following simplifing assumptions:

1. The vapor bubbles formed as a result of boiling within the flow shroud, rise with a velocity (V) given by

   $$V = V_C + V_B \tag{4}$$

   where V_C is the bulk coolant velocity without vapor production, and V_B is the bubble rise velocity resulting from buoyancy effects. Such an assumption is most valid when V_C is small.

2. The liquid-vapor two-phase mixture within the coolant shroud flows at a constant (and equal) velocity (i.e., no interfacial slip).

The average bulk coolant velocity without vapor production is given by the well-known principle

$$V_c = Q_c/A \tag{5}$$

where A is the crossectional area for flow ($A \simeq 1.698$ cm^2 for Test PR-1) and Q_c is the volumetric coolant flow rate at zero power ($Q_c \simeq 0.03$ l/s $= 30$ cm^3/s). Then, from Equation (5), $V_c \simeq 17.7$ cm/s.

The bubble rise velocity resulting from buoyancy effects (V_B) may be estimated by the expression[5]

$$V_B = 1.18 \left[\frac{\sigma g (\rho_l - \rho_v)}{\rho_l^2}\right]^{1/4} \tag{6}$$

where σ is the surface tension of the liquid and ρ_l, ρ_v are the liquid and vapor densities, respectively. Equation (6) is based on experimental observations of bubbles rising in sixteen different liquids, and has also been derived analytically.[6] For the Test PR-1 conditions[a] Equation (6) yields $V_B = 20.3$ cm/s. From Equation (4) and the calculated results of Equations (5) and (6), the total vapor velocity becomes approximately 37.96 cm/s. Therefore, from the general form of Equation (5), a total volumetric flow rate of 0.064 l/s is calculated. The calculated volumetric flow rate (0.064 l/s) compares favorably with the minimum measured volumetric flow rate (0.07 to 0.08 l/s).

4.2 Onset of Boiling Transition and Return to Nucleate Boiling

The PCM transients during Test PR-1 which resulted in detectable boiling transition are described in this section. The results are

---

a. Pressure = 15 MPa, $T_{sat} = 616$ K, $\rho_l = 0.597$ g/cm^3, $\rho_v = 0.0986$ gm/cm^3, $\sigma \simeq 64$ dyne/cm.

interpreted from the cladding elongation response of the rods via the LVDT's, since thermocouple placement was not optimized for boiling transition detection.

4.2.1 Conditions at Onset of Boiling Transition. The primary measurement for detection of boiling transition during Test PR-1 was the cladding displacement sensors (LVDT) on each rod. Following boiling transition at high pressures, the temperature excursion on the rod resulted in a change in cladding length due to thermal expansion. During a flow reduction PCM transient, this length change is readily observable. During a power increase transient, the cladding elongation response to boiling transition is somewhat confounded by the general rod elongation during the power increase. The boiling transition can usually be interpreted by a change in slope of the elongation response during a power increase transient, but is not as obvious as the response during a flow decrease. A representative LVDT response (Rod 524-3) during a boiling transition cycle is shown in Figure 14. The rapid increase in cladding displacement at about 3510 s corresponds to the onset of boiling transition, and the decrease between 3560 and 3600 s corresponds to the return to nucleate boiling (quench and rewet) process. The shroud coolant flow rate and peak test rod power are shown for reference in Figure 14. The transient corresponds to PCM Cycle 20 of Tables 4 and 7. Table 7 lists the conditions at which boiling transition was detected during the Test PR-1 PCM transients, based on the cladding displacement responses.

During many of the boiling transition cycles, instrumentation in the peak power region (0.452 m) of the rods responded to the high temperature operation. Boiling transition in vertical forced convection experiments with cosine axial power generation is generally limited to the upper rod regions except for very high heat flux and low flow rate combinations. Thermal excursions in the peak power region would, therefore, not be anticipated during the Test PR-1 transients. Thermocouple (TC) shunting in the high temperature region and possibly large temperature gradients across TC wire inhomogeneities[7] may have precipitated the observed response. Additional analysis of these effects will be required for interpretation of these data.

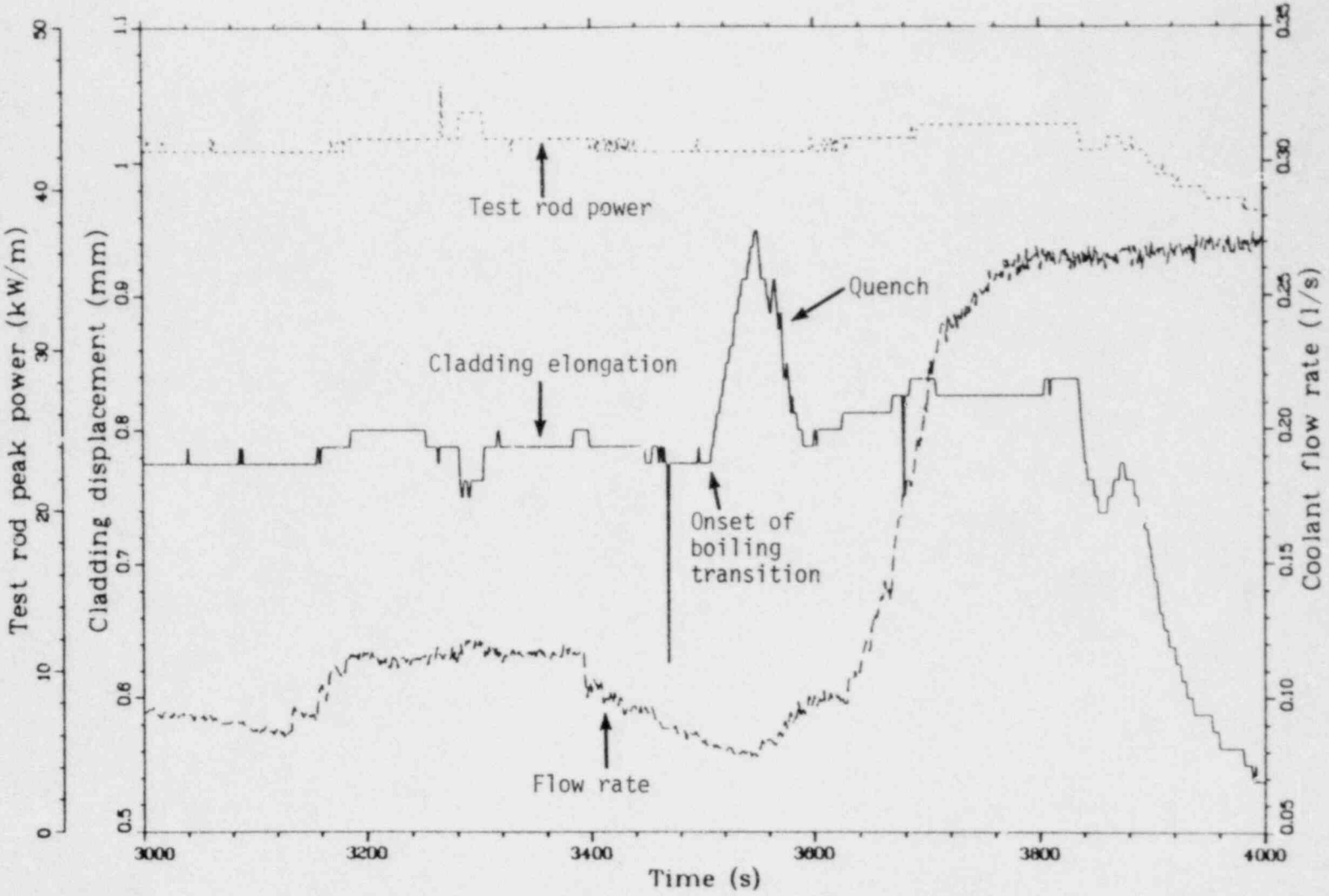

Figure 14. Representative response of LVDT to boiling transition and quench. PCM Cycle 20 (Inlet temperature = 593 K, Pressure = 12.9 MPa).

TABLE 7. BOILING TRANSITION DATA SUMMARY FOR TEST PR-1

PCM Cycle	Fuel Rod	System[a] Pressure (MPa)	Coolant Inlet[a] Temperature (K)	Peak Rod Power At Onset of BT[b] (kW/m)	Coolant Mass Flux At Onset of BT[c] (kg/m^2·s)
7	524-1	12.7	594	43.0	590
8	524-1	15.5	607	43.5	530
8	524-3	15.5	607	43.0	509
9	524-3	15.5	610	43.0	525
14	524-3	13.0	593	43.5	380
14	524-1	13.0	593	41.0	522
15	524-1	13.1	593	44.0	442
16	524-3	15.5	603	41.0	450
16	524-1	15.5	603	41.0	590
17	524-1	15.6	604	41.5	498
17	524-3	15.6	604	41.5	434
17	524-4	15.6	604	41.5	360
20	524-3	12.9	593	42.3	322
20	524-4	12.9	593	42.0	314
21	524-1	15.4	606	41.0[d]	487[d]
21	524-3	15.4	606	40.5	406
22	524-1	15.0	575	46.0[d]	890[d]
23	524-1	15.2	605	43.0[d]	550[d]
23	524-3	15.2	605	43.0	340
24	524-1	15.6	590	42.5[d]	810[d]
25	524-4	15.5	590	52.0	345

a. At start of PCM cycle.
b. Averaged (of four rods) test rod peak power at first indication of boiling transition (BT).
c. At first indication of boiling transition (BT).
d. Data from failed rod.

A direct comparison of the external cladding temperature response with the internal cladding response was possible during the Cycle 25 power increase transient. During this transient, the test rod power was increased to 53 kW/m at constant coolant flow rate (~0.1 l/s), and the flow rate subsequently reduced to about 0.075 l/s. Rod 524-4 was instrumented with thermocouples placed in small grooves on the inside cladding surface as well as external cladding surface thermocouples. Both the internal and external thermocouples at the 0.70 m elevation (from the bottom of the fuel stack) responded to the high temperature boiling transition during Cycle 25.

The measured response from the two devices is shown in Figure 15. The internal cladding thermocouple at the 0.70 m elevation consistantly indicated higher steady state temperatures (at power) than the external thermocouples, although the magnitude of the difference was consistently greater than the expected temperature drop (~67 K at 52 kW/m) across the cladding thickness. This observation suggests that fuel may have relocated to the proximity of the thermocouple junction and resulted in the higher temperature reading. Although the internal cladding temperature may be biased, the relative temperature increase and the duration of high temperature operation can be compared between the two devices.

As shown on Figure 15, the internal and external cladding temperatures on Rod 524-4 increased at nearly the same time but at different rates. The external cladding temperature increased by about 250 K within 6 s. The cladding internal temperature indicated a 210 K increase and peaked between 18 and 25 s after indication of boiling transition. The cladding external temperature measurement also exhibited different quench behavior than the internal thermocouple, apparently quenching within about 12 s of boiling transition compared to about 50 s for the internal measurement. The different behavior of internal and external cladding temperature responses during quench and rewet has been observed in other in-pile and out-of-pile tests under LOCA blowdown/reflood conditions. In general, external cladding thermocouples have been accredited with inducing earlier quenches at lower temperatures.[8] The difference in quench behavior is attributed to "fin cooling effects" on the protruding external measurement devices.

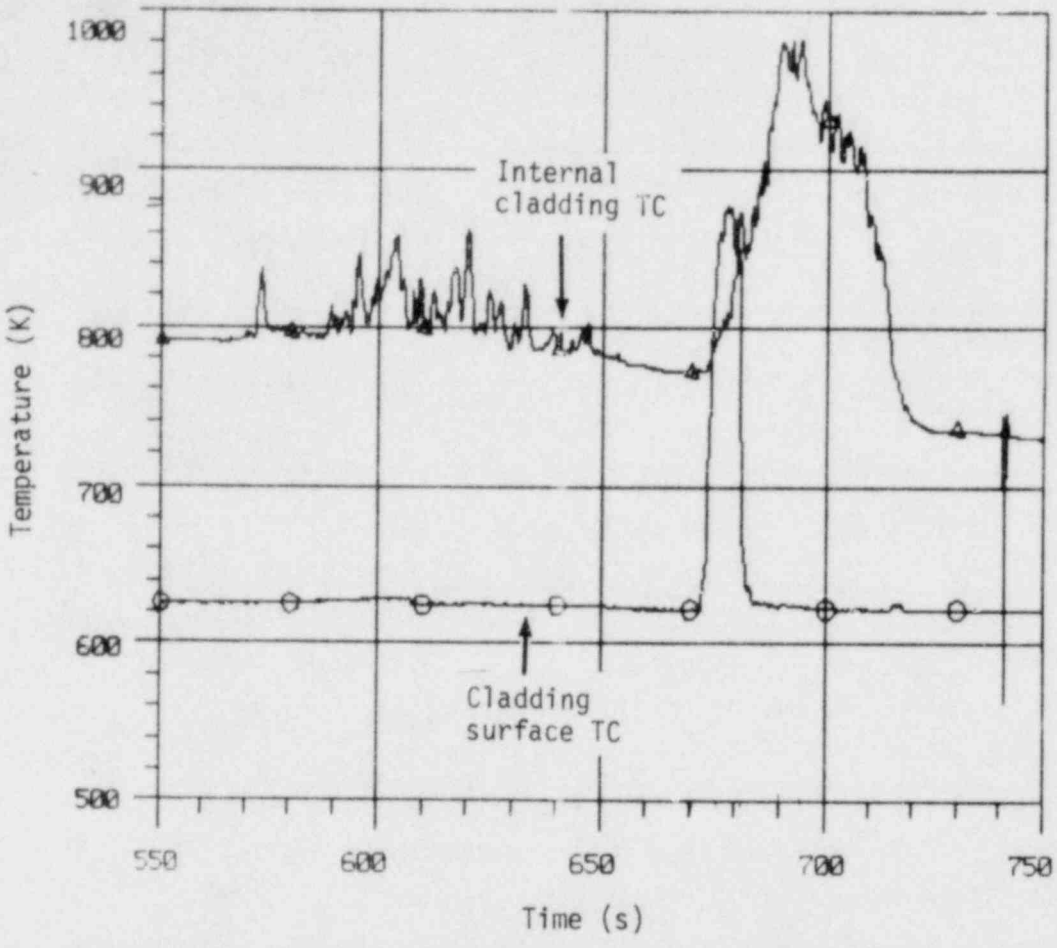

Figure 15. Internal and external cladding temperature response during PCM Cycle 25 (Rod 524-4).

The conditions at onset of boiling transition were compared to previously obtained PCM test series data on PWR-type test fuel rods. This comparison is illustrated in Figure 16. The Test PR-1 data is consistant with the trend of previous data for both the 13 and 15.5 MPa pressure conditions. The two data points from Rod 524-1 which lie outside the trend lines of previous PCM test data were obtained following rod failure. The data point for argon filled Rod 524-4 which lies outside the trend lines was obtained during PCM cycle 25. With the exception of this singular data point, inherent differences in the conditions at onset of boiling transition between the helium filled test rods and the argon filled rod were not observed.

4.2.2 Conditions at Return to Nucleate Boiling. The conditions at which return to nucleate boiling occurred were inferred from the cladding displacement response for each test rod that boiling transition was detected. The coolant conditions, coolant mass flux, and test rod power which resulted in the apparent quench of the rods are listed in Table 8. The data of Table 8 are internally consistent, with somewhat more spread in the conditions at quench than were observed from the conditions at onset of boiling transition (Table 7 and Figure 16). No significant difference in the quench behavior of the argon filled rod and the helium filled rods was apparent.

4.3 Potential for Two-Phase Instabilities

Boiling two-phase flow in a channel is inherently hydrodynamically unstable. The boiling flow in a water-cooled system is susceptible to transient flow excursions or flow oscillations due to buoyancy or compressibility effects. Such instabilities are undesirable in a reactor since they may precipitate high temperature excursions (boiling transition) of the fuel rods, induce control problems, or cause mechanical vibrations that may result in physical damage. One desirable aspect of two-phase instabilities is that they may abet quench and rewet behavior.

There are several different types of flow instabilities, many of which are interrelated. Confusion still exists within the literature regarding

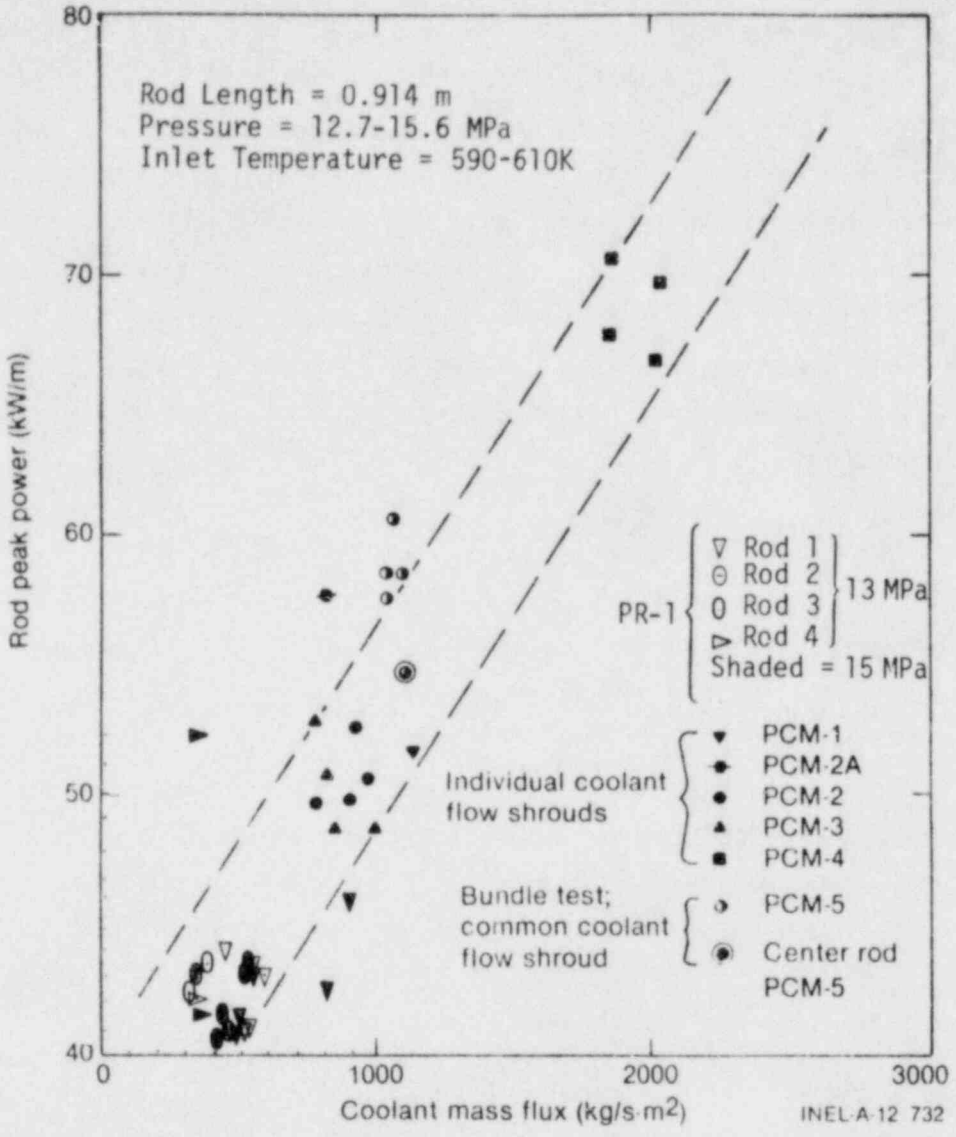

Figure 16. Comparison of the conditions at first indication of boiling transition for Test PR-1 and PCM test series.

TABLE 8. QUENCH DATA SUMMARY FOR TEST PR-1

PCM Cycle	Fuel Rod	System[a] Pressure (MPa)	Coolant Inlet[a] Temperature (K)	Peak Rod Power At Quench[b] (kW/m)	Coolant Mass Flux At Quench[b] ($kg/m^2 \cdot s$)
7	524-1	12.7	594	36.0	424
8	524-1	15.5	607	40.8	415
8	524-3	15.5	607	41.0	377
9	524-3	15.5	610	41.0	472
14	524-1	13.0	593	40.8	522
14	524-3	13.0	593	40.5	903
15	524-1	13.1	593	42.5	482
17	524-1	15.6	604	41.5	509
17	524-3	15.6	604	41.5	472
17	524-4	15.6	604	41.5	415
20	524-1	12.9	593	42.0[c]	1080[c]
21	524-1	15.4	606	39.0[c]	528[c]
21	524-3	15.4	606	39.0	467
23	524-1	15.2	606	41.5[c]	483[c]
23	524-3	15.2	606	41.2	443
24	524-1	15.6	590	43.5[c]	1096[c]
25	524-1	15.5	590	53.0[c]	426[c]
25	524-2	15.5	590	52.0	386
25	524-3	15.5	590	53.0	406
25	524-4	15.5	590	49.0	345

a. At start of PCM cycle.
b. Quench indicated by rapid drop in LVDT trace.
c. Data from failed rod.

the classification of instabilities, which is understandable since an instability can be a primary or secondary phenomenon and static or dynamic in nature. Reviews of two-phase instabilities and their classification can be found in References 9 and 10.

Two distinctly different types of instabilities were of primary concern for Test PR-1; the static flow excursion (or Ledinegg instability), and the dynamic density wave instability. Both types are considered the more likely instabilities and are more conducive for detection via the Test PR-1 instrumentation.

4.3.1 Flow Excursion (Ledinegg) Instability. The flow excursion or Ledinegg instability is characterized by a sudden change in the coolant flow rate, usually to a lower value. This type of instability occurs when the slope of channel or system demand curve becomes algebraically less than the loop or pump supply pressure drop versus flow rate curve. The criterion for this first-order, static instability, as showr in Figure 17, is given by

$$\left(\frac{\partial \Delta P}{\partial G}\right)_{\text{supply}} \geq \left(\frac{\partial \Delta P}{\partial G}\right)_{\text{system}} \qquad (7)$$

where ΔP is pressure drop, G the corresponding flow rate, and the subscripts "supply" and "system" refer to the pump or external characteristic of the channel, and system demand or internal characteristics of the channel, respectively. To satisfy the instability criterion given by Equation (7), requires that the system demand (channel characteristics) exhibit a region where the pressure drop decreases with increasing flow. Physically, this may occur when the sum of the pressure component terms: friction, acceleration, and gravity, increase with decreasing flow. Such a situation occurs, for example, for subcooled boiling of water at high fluxes[9] where increased friction and acceleration pressure drops accompany the production of nonequilibrium voids. An increase in the inlet subcooling, which decreases the channel void fraction, stabilizes the two-phase boiling flow at medium or high subcoolings (> 10 K at P $\approx$ 6 MPa) and power densities of about 50 to 75 kW/l. Conversly, lower subcoolings (<10 K at P $\approx$ 6 MPa) tend to destabilize the flow[11].

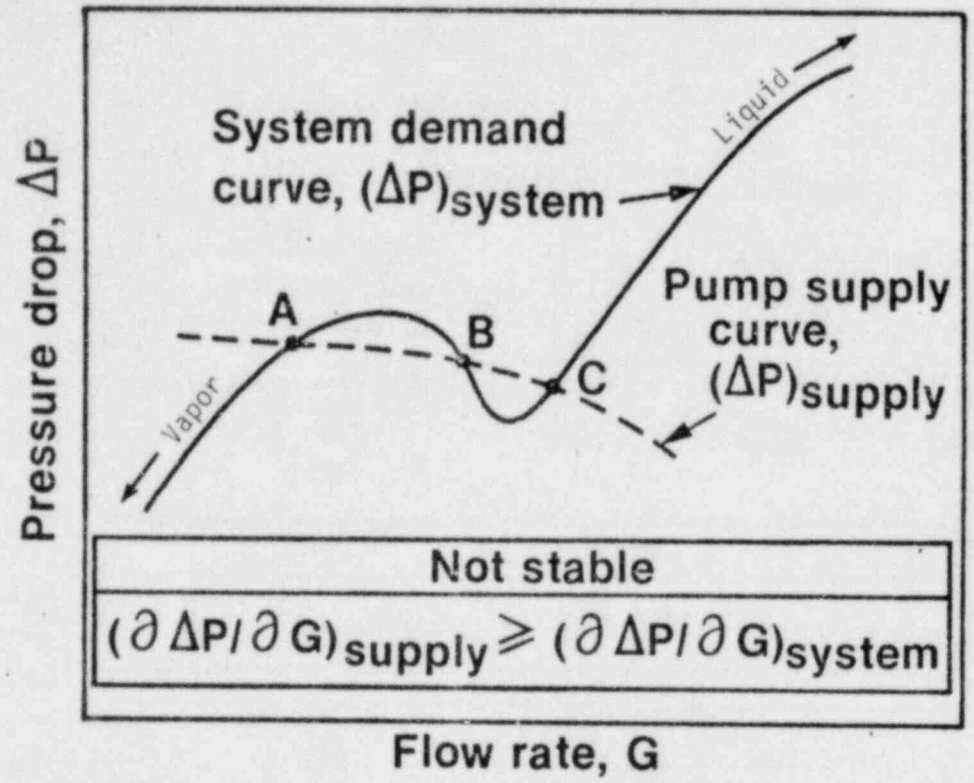

Figure 17. Qualitative illustration of criterion for flow excursion (Leninegg) instability.

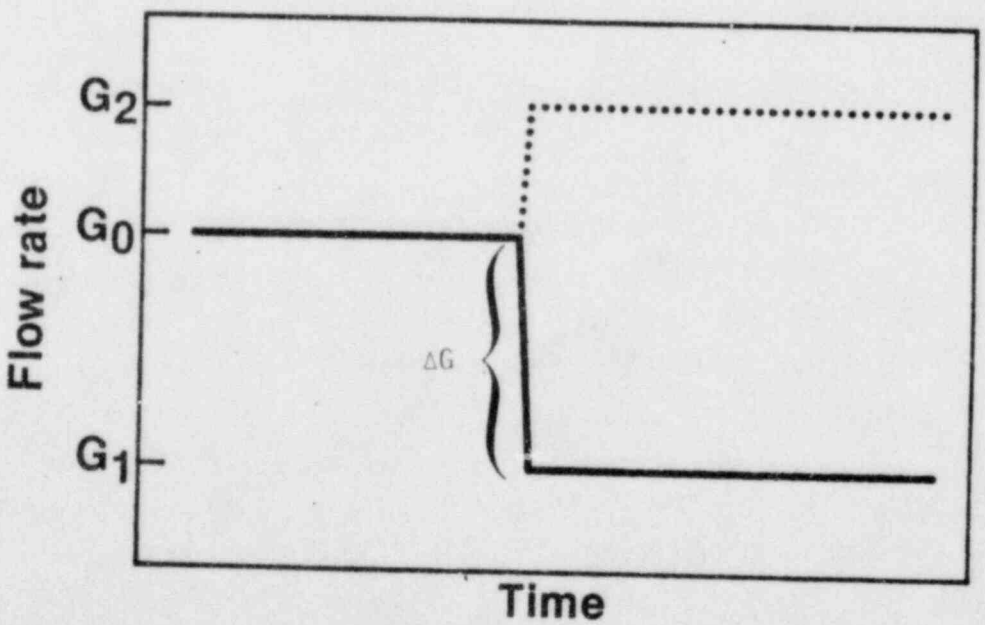

Figure 18. Conceptual illustration of the expected flow rate response should a flow excursion instability occur.

A flow excursion or Ledinegg instability is possible when a flow perturbation occurs at a hydrodynamically unstable state. Qualitatively, as illustrated in Figure 17, such an excursion can occur during a flow reduction where the system demand curve begins to overburden the pump supply curve (Point C, Figure 17). Since the pump cannot overcome the friction requirements of the system, the flow is further reduced. The excursion continues along the pump supply curve until a new stable flow rate is established at the intersection of the pump supply and system demand curves (Point A, Figure 17)[9]. Such an excursion may lead to premature boiling transition and momentarily disrupts the thermal hydraulics of the system.

Theoretically, the characteristics of a flow excursion instability may be quantified. In practice, however, complex geometries and rigorous nonequilibrium two-phase flow modeling make such calculations arduous. For Test PR-1, primary emphasis was therefore placed on the detection, rather than prediction, of the flow excursion (Ledinegg) instability. Pressure drop measurements across individual coolant flow shrouds, in conjunction with continuous monitoring of coolant flow rates and wide variety of coolant-pressure-power test parameters increase the potential for detection of a flow excursion instability, should one occur.

Figure 18 conceptually illustrates the expected coolant flow rate versus time behavior should a flow excursion instability occur. During a flow decrease, the coolant flow rate would take a marked drop from an initial flow value of G_0 to some hydrodynamically stable lower flow rate value of G_1. Such a change in the coolant flow rate ($\Delta G = G_0 - G_1$) may be viewed as going from Point C to Point A in Figure 17. If the system demand curve (Figure 17) is quantitatively known, the magnitude of the excursive flow rate change (ΔG, see Figure 18) can be estimated.

When a number of flow channels having common inlet and outlet plenums operate hydraulically in parallel, all have the same pressure drop. This is true for the Test PR-1 geometry. The pressure difference measurements (ΔP) across Rod 524-3 and -4 flow shrouds are therefore representative of the pressure difference (measured at the same elevations) elsewhere within the test system.

Figure 19 illustrates the pressure differential (ΔP) across flow shroud number 3 as a function of coolant flow rate (G) for the high pressure PCM cycle number 16. The curve (loop) illustrated corresponds to the observed behavior during the flow reduction and subsequent flow increase periods. Also shown are the approximate points where the onset of boiling and boiling transition occurred, and a generalized system demand curve. From this Figure, several observations are made:

1. During the period of flow decrease, the experimentally measured ΔP versus G trace (solid line) follows a generalized system demand curve (dashed line).

2. The power/coolant conditions during this PCM cycle (cycle 16) were such that the high quality (vapor) region of the system demand curve was not attained.

3. The ΔP vs G curve is continuous and does not exhibit flow excursion characteristics. This in itself may be interpreted as the absence of a flow excursion (Ledinegg) instability for the conditions illustrated.

4. When the coolant flow rate was increased (following boiling transition) the ΔP vs. G trace exhibits hysteresis and does not return to a single-phase liquid state via the same path. Such behavior may be viewed as a fundamental difference in the onset of boiling and return to no-boiling conditions. Mathematically, the interdepencency of the friction, acceleration and gravity pressure drop components, and the coolant flow rate (G) may provide insight into such behavior.

As previously discussed, should a flow excursion instability be present, a distinct flow rate change (ΔG) would be expected (Figure 18). Figure 20 illustrates the coolant flow rates (flow Shrouds -3 and -4) versus time typically measured during periods of flow reduction for Test PR-1. As shown, there are no positive indications that a flow excursive (Ledinegg) instability occurred.

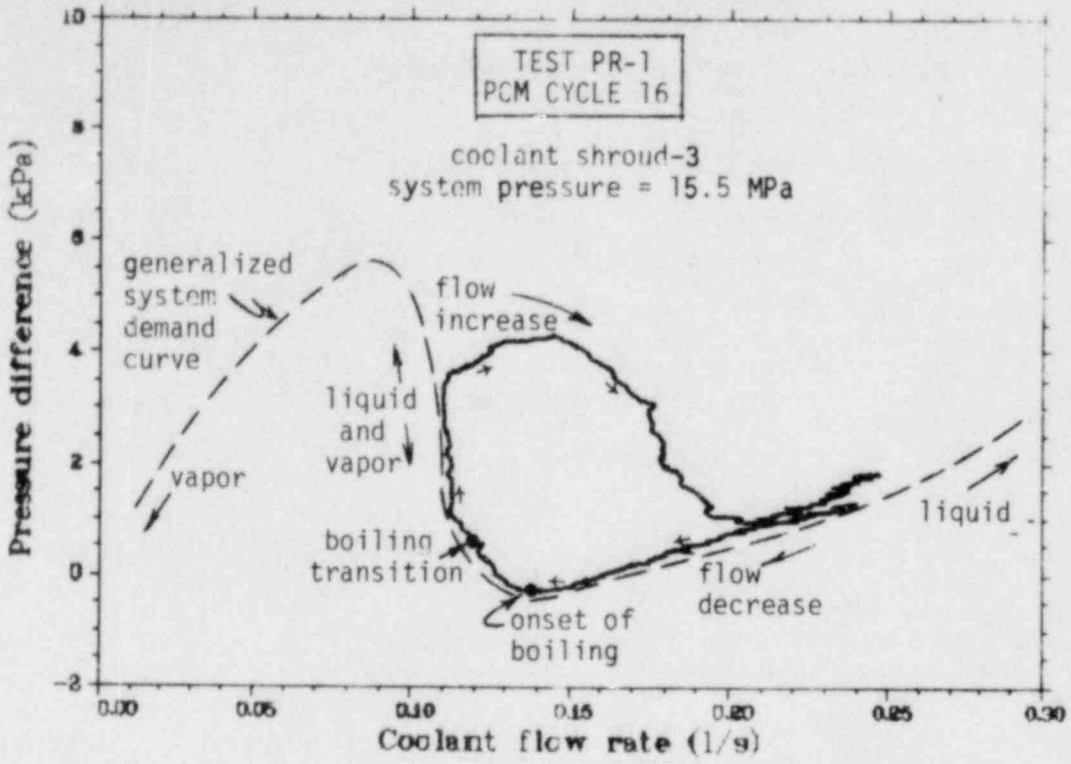

Figure 19. Measured pressure drop as a function of coolant flow rate for Rod 524-3 during flow reduction and increase cycle.

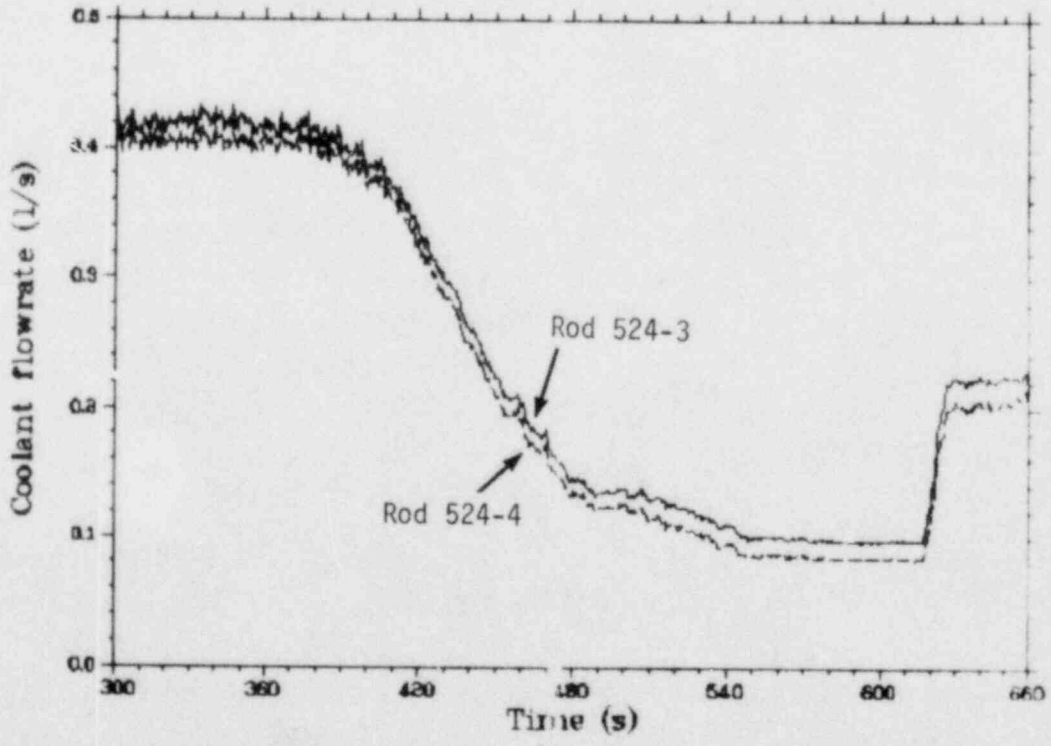

Figure 20. Coolant flow rate for Rods 524-3 and 524-4 typically measured during periods of flow reduction showing no observable flow excursion instabilities.

4.3.2 Density Wave Instability. The second type of two-phase instability of primary interest in Test PR-1 was the dynamic density wave instability. This type of instability is generally considered the most common, and has been widely observed in boiling equipment over past years.[12]

Figure 21 illustrates the mechanism for a density wave instability. If the inlet coolant flow rate is momentarily decreased, vapor production within the flow shroud increases. The resultant lower density two-phase mixture within the flow shroud gives rise to an increase in the discharge velocity which, in turn, leads to water accumulation within the shroud. When the higher density mixture arrives at a downstream exit with some imposed resistance, the discharge velocity decreases and the cycle starts again. The frequency of this cycle depends on the vapor production rate and the propagation velocity of the density disturbances.

Theoretically, the potential for a density wave instability in a boiling channel may be estimated by a simplified stability criterion of Saha, et al.[11]

$$N_{pch,eq} - N_{sub} = \frac{2\left[K_i + \frac{f_m}{2D_h} + K_e\right]}{1 + 1/2\left[\frac{f_m}{2D_h} + 2K_e\right]} \qquad (8)$$

where $N_{pch,eq}$ is an equilibrium phase change number (power dependent), N_{sub} a subcooling number, f_m a two-phase mixture friction factor, D_h the hydraulic diameter and K_i and K_e are inlet and outlet resistance coefficients, respectively. Equation (8) is based on a thermal equilibrium model, and has been successfully demonstrated out-of-pile.

Application of equation (8) to the Test PR-1 conditions is difficult. In particular, the outlet resistance coefficient (K_e), which requires precise modeling of the outlet resistance, is not known. Downstream instrumentation, lead wires, flow screens, and several minor flow channel expansions and contractions make estimation of the resistance complex. Therefore, as with the excursive instability, primary emphasis was placed on detection, rather than prediction, of density wave instabilities.

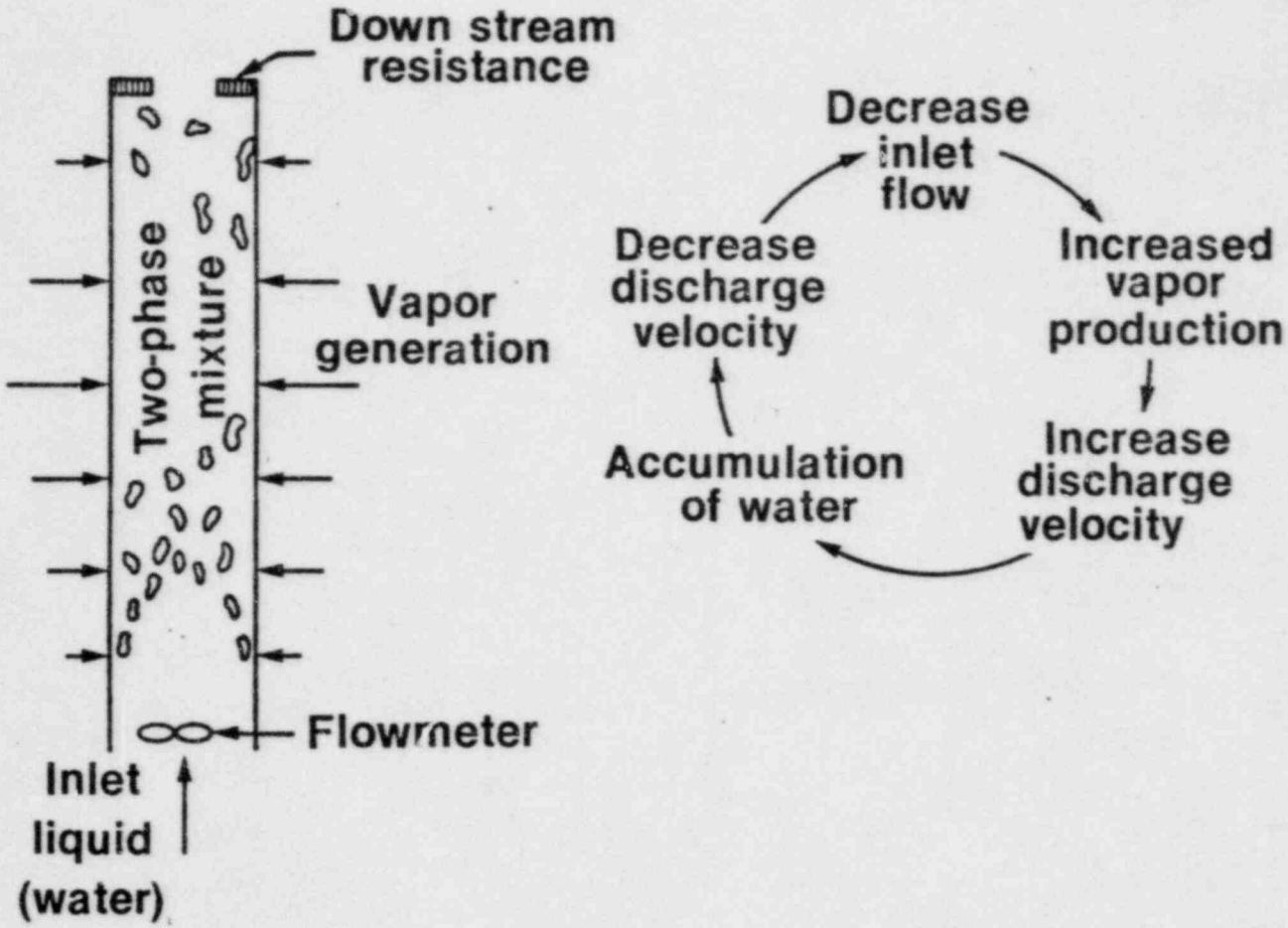

Figure 21. Illustration of the mechani:m for density wave instabilities.

Figure 22 illustrates a method for detecting a density wave instability. Should such an instability occur, the shroud coolant flow and pressure differential (ΔP) responses would oscillate around a mean value with a constant period (τ). If power is increased during a period of instability, the flow rate and pressure differential oscillations would be expected to increase in amplitude, but maintain approximately the same period. The period of oscillation (τ) is proportional to the propagation velocity of the density disturbances and, for a first estimate, it can be assumed that the density disturbance travels at the coolant velocity. For a typical coolant flow rate of 0.1 l/s within an individual coolant flow shroud, the coolant velocity (liquid phase) is about 60 cm/s. Since the flow shroud is a little over a meter long, oscillations with a period on the order of 1.5 to 2 seconds would be expected.

Figure 23 illustrates the coolant flow rate and pressure differential versus time experimentally measured during a typical PCM cycle. As shown, there is no evidence of coolant or pressure fluctuations indicitive of a density wave instability.

In summary, preliminary analysis of the Test PR-1 experimental data indicates no positive indication of either a flow excursion (Ledinegg) or density wave two-phase instability. Such an observation is consistant with the experimental results of previous out-of-pile investigations, (Reference 7-11) where higher system pressures reduce the potiential for two-phase instabilities.

1. Flowmeter

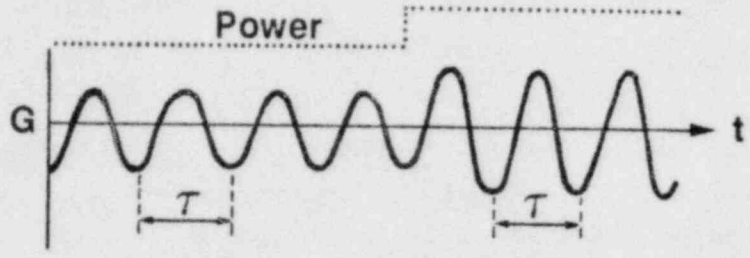

2. ΔP transducers

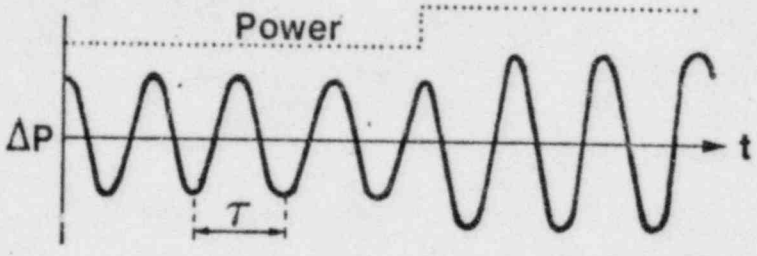

Figure 22. Expected pressure drop and flow rate responses should a density wave instability occur.

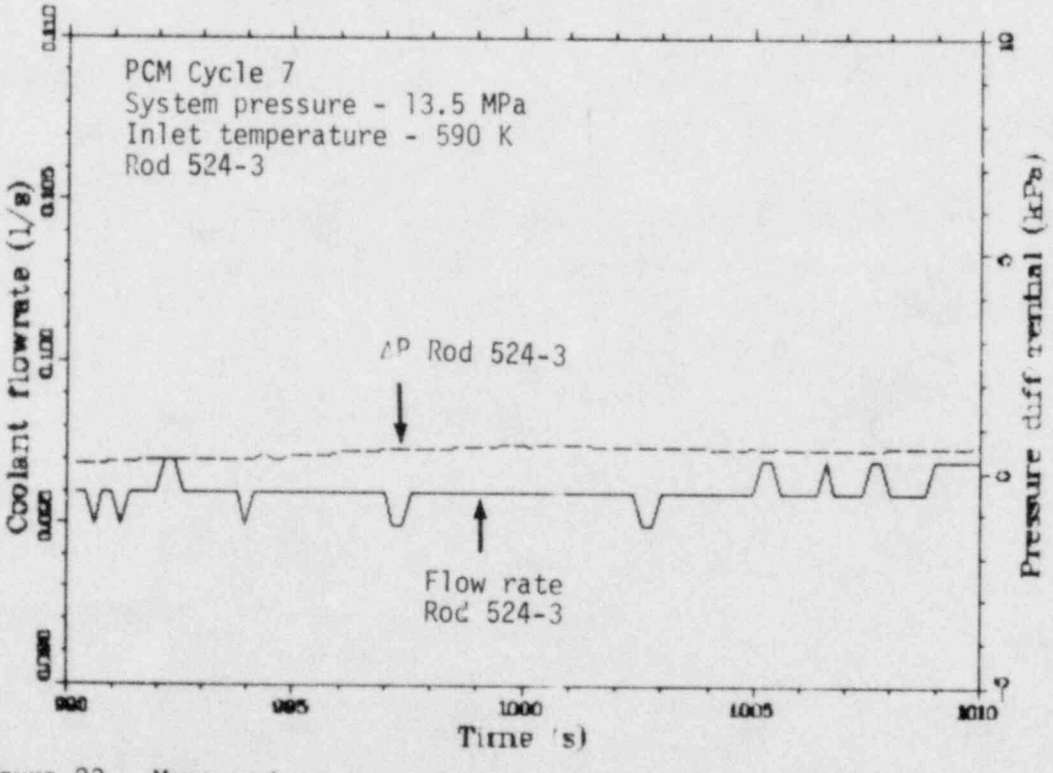

Figure 23. Measured pressure drop and flow rate during a typical PCM cycle showing no observable density wave instabilities.

5. RIA POWER EXCURSION RESULTS

Three power bursts were conducted during Test PR-1. Rods 524-2 and 524-3 failed during the power bursts. The reactor and test rod energy data for the three power bursts are summarized in Table 9. The maximum values for the measured cladding and fuel temperatures, cladding elongation change, and internal rod pressure change are listed in Table 10. The results for each power burst are discussed below.

5.1 Power Burst-1

A radial average fuel enthalpy at the axial peak elevation of 105 cal/g UO_2 (125 cal/g UO_2 peak local fuel enthalpy at the fuel centerline) was achieved in the first power burst. The maximum cladding surface temperature measured on the four rods was 875 K on Rod 524-2. High temperature film boiling occurred for about 2 s. Maximum fuel temperatures of 2140 and 1630 K were measured by the fuel centerline and off-center thermocouples, respectively. Two of the four fuel centerline thermocouples and six of the twelve off-center fuel thermocouples were operable during the power burst. As indicated by the internal rod pressure transducer, Rod 524-1 failed during previous PCM testing. During the burst, the internal pressure transducer on this rod indicated a pressure pulse increase of 1.2 MPa due to steam formation in this water-logged fuel rod. Coolant pressure increases of 0.4 MPa were recorded by the system pressure transducers. No indications of an additional rod failure were observed. No significant changes in the figure-of-merit for any of the four fuel rods were measured during the steady-state power calibration performed following the power burst.

A comparison between measured and FRAP-T5[a] predicted fuel centerline temperatures for Rod 524-2 during Power Burst-1 is shown in Figure 24. A similar comparison between measured and predicted off-center fuel temperatures is shown in Figure 25. During the initial temperature increase, the predicted

---

a. FRAP-T5, Idaho National Engineering Laboratory Configuration Control Number H0175828.

TABLE 9. TEST PR-1 POWER BURST ENERGY DATA

Power Burst Number	Reactor Period (ms)	Peak Reactor Power (MW)	Reactor Energy Release to Time of Scram (MJ)	Test Fuel Rod Total Energy (cal/g UO_2)	Radial Average Peak Fuel Enthalpy (cal/g UO_2)	Peak Local Fuel Enthalpy (cal/g UO_2)
1	42.7	130	110	170	105	125
2	8.7	2650	112	175	125	135
3	6.2	5700	158	245	180	205

TABLE 10. MAXIMUM MEASURED FUEL ROD PARAMETERS DURING TEST PR-1 POWER EXCURSIONS

Power Burst Number	Test Rod Number	Maximum Cladding Temperature (K)	Maximum Fuel Centerline Temperature (K)	Maximum Fuel Off-center Temperature (K)	Maximum Cladding Elongation Change (mm)	Maximum Internal Rod Pressure (MPa)
1	524-1	795	1120	1425	2.6	1.2 Pulse
1	524-2	875	2140	1625	2.5	2.6
1	524-3	760	(X)	1575	2.0	(X)
1	524-4	995	(X)	1630	2.1	1.3
2	524-1	1165	1065	1250	Rod Separated	5.5 Pulse
2	524-2	1180	2220	(X)	5.8	2.7
2	524-3	1345	(X)	(X)	Rod Separated	(X)
2	524-4	1180	(X)	1980	4.5	1.3
3	524-1	1970	(X)	1825	Rod Separated	6.7 Pulse
3	524-2	1615	2750	(X)	8.7	3.35; Rod Failed
3	524-3	1970	(X)	(X)	Rod Separated	(X)
3	524-4	1290	(X)	(X)	7.8	1.55

(X) Indicates failed instrument(s).

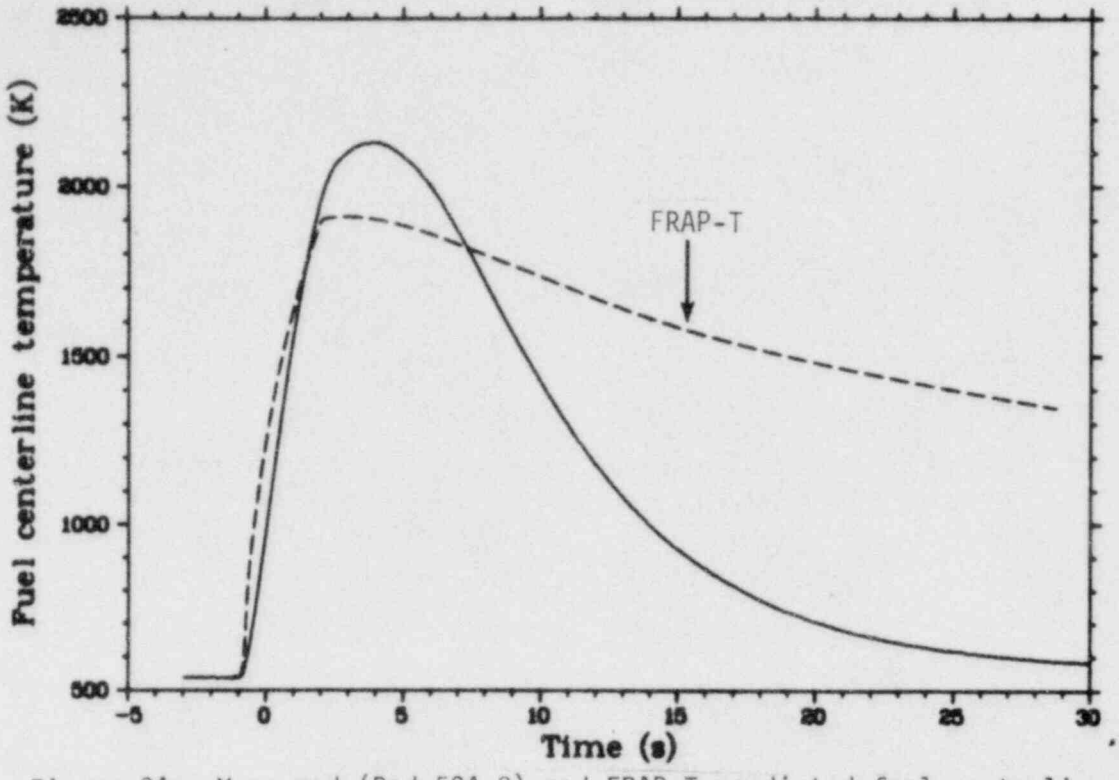

Figure 24. Measured (Rod 524-2) and FRAP-T predicted fuel centerline temperatures during Power Burst-1.

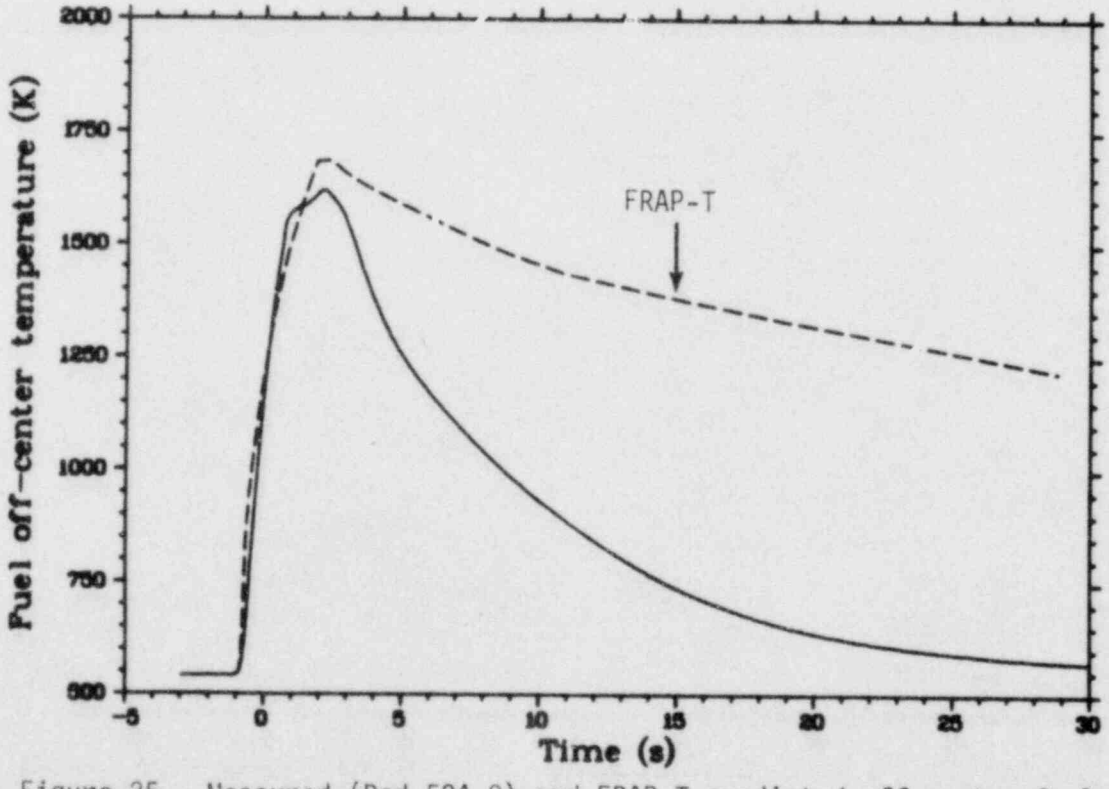

Figure 25. Measured (Rod 524-2) and FRAP-T predicted off-center fuel temperatures during Power Burst-1.

centerline temperature increases slightly faster than the measured temperature. The measured and predicted off-center temperatures are nearly identical. The measured centerline temperature was about 210 K higher than the prediction, and the measured off-center temperature peak about 75 K less than predicted by FRAP-T. The noteable difference in the measured and predicted fuel temperature response is the rate at which the rod is cooled. The predictions suggest that the fuel temperatures will remain higher for an appreciable time longer than were measured. Both fuel temperature measurements indicated nearly pre-transient temperatures in the time frame of the calculation (30 s). This implies that the calculations using FRAP-T may be conservatively predicting the fuel damage as a consequence of this relatively low energy power burst.

5.2 Power Burst-2

A radial average fuel enthalpy at the axial peak elevation of 125 cal/g UO_2 (135 cal/g UO_2 peak local fuel enthalpy near the pellet surface) was reached in the second power burst. The maximum measured cladding surface temperature was 1345 K on Rod 524-3. Film boiling occurred for about 7 s. Maximum fuel temperatures of 2220 and 1980 K were measured by the fuel centerline and off-center fuel thermocouples, respectively. Two of the fuel centerline and two off-center fuel thermocouples were operable during the power burst. The internal pressure transducer on Rod 524-1 indicated a 5.5 MPa pressure pulse due to steam formation in this rod. A loop pressure increase of about 0.6 MPa was measured by the system coolant pressure transducers.

The LVDT for Rod 524-3 indicated that this rod probably fractured during the second power burst. The internal pressure transducer for this rod had been inoperable since the beginning of the test so rod failure could not be confirmed. The LVDT for Rod 524-1 also indicated that this rod completely fractured during the burst. No significant changes in the figure-of-merit for any of the four fuel rods were measured during the steady-state power calibration performed after the second power burst.

The measured and FRAP-T5 predicted fuel centerline temperatures during the second power burst are shown in Figure 26. The predicted temperature rise

is somewhat faster than the measured increase, a result which might be expected due to the inherent delay time in the centerline thermocouple response. The measured peak temperature of about 2220 K agrees well with the predicted maximum of 2240 K. As was observed during Power Burst-1, the measured centerline cooling rate was significantly faster than predicted over the time range of the calculation (30 s).

5.3 Power Burst-3

A radial average fuel enthalpy at the axial peak elevation of 180 cal/g UO_2 (205 cal/g UO_2 peak local fuel enthalpy near the pellet surface) was reached in the third power burst. The maximum measured cladding surface temperatures were 1970 K on Rods 524-1 and 524-3. Film boiling occurred for about 11 s. Maximum fuel temperatures of 2750 and 1825 K were measured by the fuel centerline and off-center fuel thermocouples, respectively. Only one fuel centerline and one off-center fuel thermocouple were operable during the third power burst.

The internal pressure transducer on Rod 524-1 indicated a 6.7 MPa pressure pulse due to steam formation in this rod. A loop pressure increase of about 0.9 MPa was measured by the system coolant pressure transducers. The flowmeter for Rod 524-1 indicated zero shroud flow after the power burst.

The internal pressure transducer for Rod 524-2 indicated that this rod failed about 2.5 s after the time of peak power. The cladding surface thermocouple located at 452 mm (180°) indicated a temperature of 1550 K at this time.

The measured centerline fuel temperature for Rod 524-2 is shown compared to the FRAP-T prediction in Figure 27. The predicted temperature again increases faster than the measured temperature during the initial temperature rise. Failure of the test rod was predicted for Power Burst-3 due to the cladding strain rate, at a time corresponding to about 70 ms following peak power. As noted above, an indication of failure on Rod 524-2 was observed about 2.5 s after peak power.

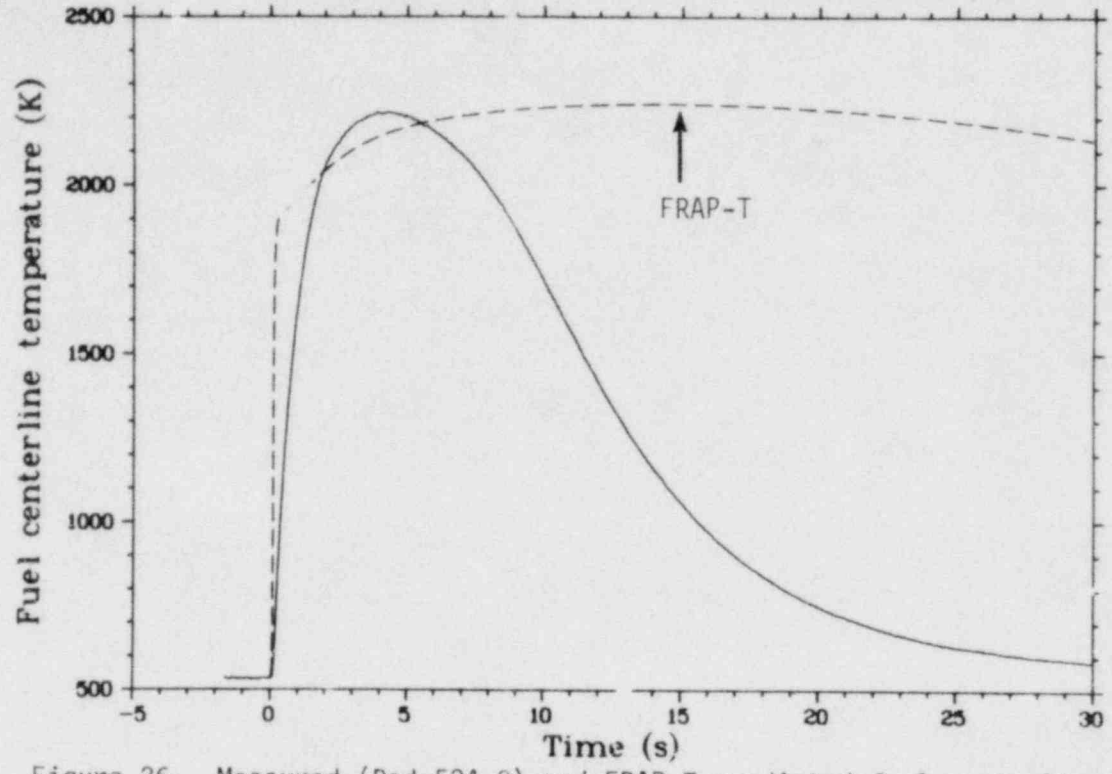

Figure 26. Measured (Rod 524-2) and FRAP-T predicted fuel centerline temperatures during Power Burst-2.

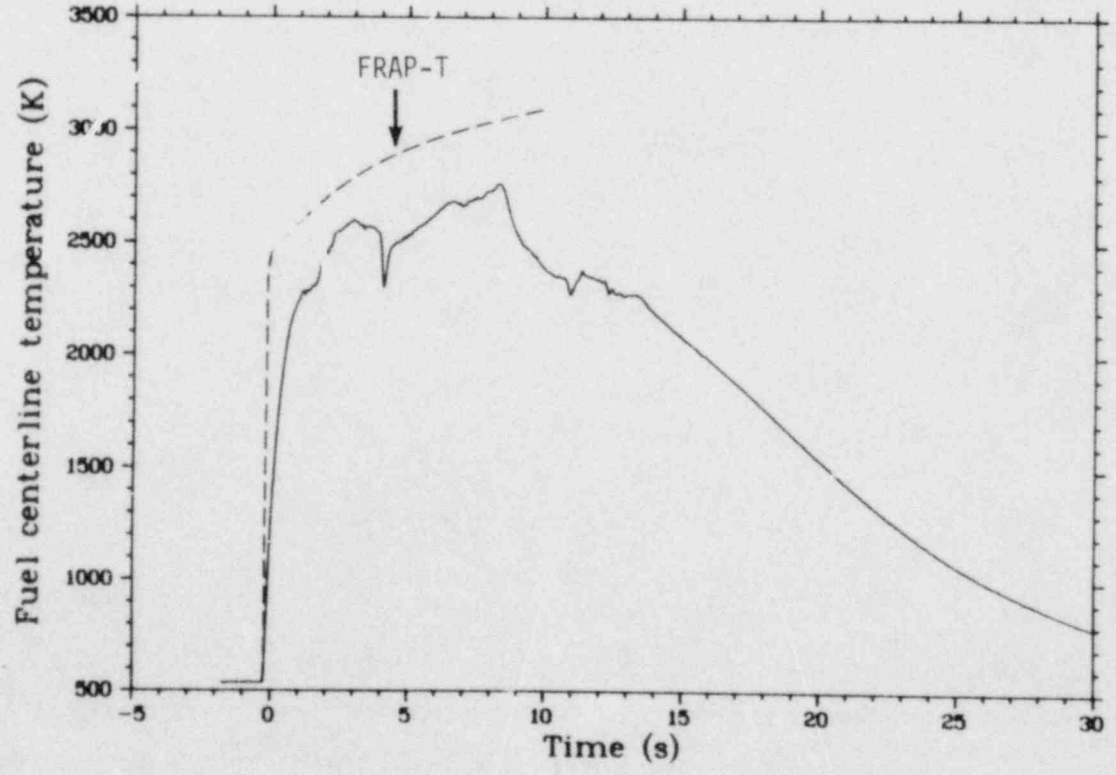

Figure 27. Measured (Rod 524-2) and FRAP-T predicted fuel centerline temperatures during Power Burst-3.

5.4 Power Burst Summary

Rods 524-3 and 524-2 failed during the power burst testing at radial average peak fuel enthalpies of 125 and 180 cal/g UO_2, respectively. Rod 524-2 had experienced only a short duration (~60 s) of high temperature operation during the PCM test phase. Rod 524-4, which was the only rod back-filled with argon, did not fail during the power burst testing. The maximum measured cladding temperature for Rod 524-4 during the three bursts was 1290 K, about 700 K less than that measured for the other three rods. However, during the lowest energy burst, measured cladding temperatures on Rod 524-4 were between 120 and 235 K higher than the helium filled test rod temperatures.

Rapid steam formation in previously failed Rod 524-1 produced very sharp pressure pulses during each power burst. This is the first known power burst testing of a water-logged fuel rod at typical operating temperatures and pressures. In Power Burst-3, the source pressure pulse of 6.7 MPa was attenuated to about 0.9 MPa at the location of the system coolant pressure transducers (above the shroud outlets). As evidenced by the power calibration checks made after Power Bursts-1 and -2, no significant amount of fuel was expelled from the Rod 524-1 flow shroud. This indicates that the fuel pellets in the water-logged rod did not fragment into small particles during the first two power bursts.

6. SUMMARY OF RESULTS AND DISCUSSION

The primary Test PR-1 objectives included; obtaining fuel rod thermal response data under steady state and power oscillation conditions, evaluating the conditions at onset of boiling transition and return to nucleate boiling, and providing data on fuel temperature distributions and fuel failure limits during RIA power excursions. The following results and observations are based on a preliminary evaluation of the Test PR-1 data.

1. Fuel rod thermal response data obtained during the Test PR-1 steady state operation was consistent with results from the Gap Conductance Test Series on similar design fuel rods. The effect of fuel density upon centerline and off-center fuel temperatures was minimal when compared to the much larger effect of fill gas composition (helium or argon).

2. For the helium filled test rods, the measured centerline temperatures agreed well with predictions using the (FRAP-T) free thermal expansion fuel model. Off-center fuel temperature measurements agreed well with predicted temperatures using the Coleman relocation fuel model. Centerline temperatures for the argon filled test rod were overpredicted by the free thermal expansion model and under predicted by the Coleman relocation fuel model. Neither model reflected the trend of limited off-center fuel temperature data in the argon filled rod.

3. Large differences between gap conductance values obtained by the power oscillation and $\int k dT$ methods were observed. Values obtained by the power oscillation method were inconsistent and often unrealistic. The method is apparently inconsistent, either due to non-linearities in fuel conductivity and gap conductance, or intermittant pellet and cladding contact during the power oscillations.

4. The conditions at onset of boiling transition and return to nucleate boiling were evaluated at coolant pressures between 13 and

15.5 MPa. The boiling transition data were consistent with trends obtained from previous PCM tests on PWR rods at similar pressures. Boiling transition at BWR pressures was not observed. Natural circulation apparently limited the minimum flow rate that could be achieved in the Test PR-1 geometry. A low temperature excursion associated with high quality boiling transition may have occurred but was not detectable.

5. Rod 524-1 failed following several minutes of intermittent high temperature operation. The likely cause of failure was extensive embrittlement. In contrast, a positive indication of boiling transition on Rod 524-2 was observed only once during the PCM testing (~ 60 s duration). Measured coolant conditions for each test rod were essentially identical. The possibility of interactive hydraulic coupling of the rods through the common upper and lower plenums will be investigated in subsequent analysis.

6. The potential for two-phase flow instabilities was investigated during Test PR-1. Preliminary analysis of the data indicated no positive evidence of either a two-phase flow excursion (Ledinegg) or density wave instability.

7. RIA power bursts were conducted which resulted in radial averaged fuel enthalpies (at the axial peak location) of 105, 125, and 180 cal/g UO_2. Rod 524-3 likely failed during the second (125 cal/g UO_2) power burst as evidenced by a sharp decrease in elongation shortly following the burst. Rod 524-2 failed during the third (180 cal/g UO_2) power burst, about 2.5 s after peak power. Rod 524-4, the only argon filled test rod, experienced maximum cladding temperatures about 700 K less than the helium filled rods, and did not fail during the burst testing.

8. Rod 524-1 was waterlogged for the burst testing since it had previously failed during the PCM transient test phase. The rod internal pressure transducer for this rod indicated pressure pulses of 1.2, 5.5 and 6.7 MPa during the three progressively severe power

excursions. The pressure pulses were attenuated rapidly and resulted in system pressure increases (measured near the shroud outlets) of 0.4, 0.6 and 0.9 MPa, respectively.

9. Maximum fuel and cladding temperatures were attained following the third power excursion. The maximum measured fuel centerline, off-center fuel, and cladding surface temperatures during the third burst were 2750, 1925 and 1550 K, respectively.

REFERENCES

1. R. W. Garner, et al., Gap Conductance Test Series-2 Test Results Report for Tests GC 2-1, GC 2-2, and GC 2-3, NUREG/CR-0300, TREE 1268, November 1978.

2. R. H. Smith, Power Cooling Mismatch Test Series, Test PR-1 Experiment Predictions, EGG-TFBP-5056, January 1980.

3. D. N. Plummer, et al. "Post Critical Heat Transfer to Flowing Liquid in a Vertical Tube," MIT Report 72718-91, Massachusetts Institute of Technology (1974).

4. M. M. El-Wakil, Nuclear Heat Transport, International Textbook Co, pp. 412-417 (1971).

5. F. N. Peebles and H. J. Garber, "Studies on the Motion of Gas Bubbles in Liquids," Chemical Engineering Progress, Vol. 49, No. 2, 1953, pp 88-97.

6. S. S. Kutateladze and M. A. Styrtkovich, Hydraulics of Liquid-Air Systems, Gosenereoizdat, Moscow 1958.

7. R. J. Moffat, Experimental Methods in the Thermosciences, Department of Mechanical Engineering, Stanford University (1978).

8. F. S. Gunnerson, "On the Prediction of Quench and Rewet Temperatures," To be Published in Proceedings of ANS Annual Meeting, Las Vegas, Nevada June 1980.

9. J. A. Boure, A. E. Bergles and L. S. Tong, "Review of Two-Phase Flow Instability," Nuclear Engineering and Design, 25, 1973, pp 165-192.

10. A. E. Bergles, "Review of Instabilities in Two-Phase Systems," Two-Phase Flows and Heat Transfer, edited by S. Kakac and F. Mayinger, Vol. 1 1974, pp. 383-422.

11. R. P. Mathisen, "Out-of-Pile Channel Instability in the Loop Skalvan," Symposium on Two-Phase Dynamics, Eindhoven, September 1967.

12. Y. Y. Hsu and R. W. Graham, Transport Processes in Boiling and Two-Phase Systems, McGraw-Hill, 1976, Chapter 9.

13. P. Saha, M. Ishii and N. Zuber, "An Experimental Investigation of Thermally Induced Flow Oscillations in Two-Phase Systems," Journal of Heat Transfer, November 1976, pp 616-622.